

Spring 4-2011

## Porous Metal-Organic Materials by Design Using Neutral Organic Ligands

Stephen Burd  
*University of South Florida*

Follow this and additional works at: [https://digitalcommons.usf.edu/honors\\_et](https://digitalcommons.usf.edu/honors_et)



Part of the [American Studies Commons](#)

---

### Scholar Commons Citation

Burd, Stephen, "Porous Metal-Organic Materials by Design Using Neutral Organic Ligands" (2011).  
*Outstanding Honors Theses*. 13.  
[https://digitalcommons.usf.edu/honors\\_et/13](https://digitalcommons.usf.edu/honors_et/13)

This Thesis is brought to you for free and open access by the Honors College at Digital Commons @ University of South Florida. It has been accepted for inclusion in Outstanding Honors Theses by an authorized administrator of Digital Commons @ University of South Florida. For more information, please contact [digitalcommons@usf.edu](mailto:digitalcommons@usf.edu).

**Porous Metal-Organic Materials by Design Using Neutral  
Organic Ligands**

**by**

**Stephen Burd**

A thesis submitted to the USF Honors College  
in conformity with the requirements  
for the degree of Honors

University of South Florida

Department of Chemistry

April 2011



I would like to thank my family for their continued support and love for me throughout my life and education.

I would like to thank Jason A. Perman for his guidance and patience in developing this project. I would also like to thank Dr. Michael Zaworotko for giving me the opportunity and time to perform this project.

## **Chapter 1 – Introduction**

<b>1.1 Preamble</b>	1
<b>1.2 Supramolecular Chemistry</b>	
1.2.1 Supramolecular History	2
1.2.2 The Noncovalent Bond	2
<b>1.3 Crystal Engineering</b>	
1.3.1 History of Crystal Engineering	4
<b>1.4 Metal-Organic Materials</b>	
1.4.1 Introduction to the Metal-Organic Material	4
1.4.2 History of the MOM	5
1.4.3 Properties of MOMs	6
1.4.3.1 <i>The 4,4'-bipyridyl linker and its impact</i>	6

## **Chapter 2 – Synthesis of Three Isorecticular MOMs**

<b>2.1 Introduction</b>	10
<b>2.2 Synthesis of [Cu(4,4'-bipyridyl)<sub>2</sub>SiF<sub>6</sub>]<sub>n</sub></b>	11
<b>2.3 Synthesis of [Cu(1,2-Di(4-pyridyl)ethylene)<sub>2</sub>SiF<sub>6</sub>]<sub>n</sub></b>	
2.3.1 {[Cu(1,2-Di(4-pyridyl)ethylene) <sub>2</sub> (H <sub>2</sub> O) <sub>2</sub> ](SiF <sub>6</sub> )(H <sub>2</sub> O)} <sub>n</sub>	13
2.3.2 [Cu(1,2-Di(4-pyridyl)ethylene) <sub>2</sub> SiF <sub>6</sub> ] <sub>n</sub>	16
<b>2.4 Synthesis of [Cu(pyrazine)<sub>2</sub>SiF<sub>6</sub>]<sub>n</sub></b>	
2.4.1 [Cu(pyrazine)(SiF <sub>6</sub> )(H <sub>2</sub> O) <sub>2</sub> ] <sub>n</sub>	18
2.4.2 Cu(3,5-lutidine) <sub>4</sub> SiF <sub>6</sub>	19

2.4.3 [Cu(pyrazine) <sub>2</sub> (SiF <sub>6</sub> )(H <sub>2</sub> O)] <sub>n</sub>	20
2.4.4 [Cu(pyrazine) <sub>2</sub> SiF <sub>6</sub> ] <sub>n</sub>	22
<b>2.5 Properties of Synthesized MOMs</b>	
2.5.1 Thermal Gravimetric Analysis	25
2.5.2 Bond Distances and Window Size	26
2.5.3 Determination of Surface Area from Nitrogen Isotherms	27
<b>2.6 Discussion</b>	28
<b>2.7 Experimental</b>	
2.7.1 Synthesis of [Cu(4,4'-bipyridine) <sub>2</sub> SiF <sub>6</sub> ] <sub>n</sub>	30
2.7.2 Synthesis of {[Cu(1,2-Di(4-pyridyl)ethylene) <sub>2</sub> (H <sub>2</sub> O) <sub>2</sub> ](SiF <sub>6</sub> )(H <sub>2</sub> O)}	30
2.7.3 Synthesis of [Cu(1,2-Di(4-pyridyl)ethylene) <sub>2</sub> SiF <sub>6</sub> ] <sub>n</sub>	30
2.7.4 Synthesis of [Cu(pyrazine)(SiF <sub>6</sub> )(H <sub>2</sub> O) <sub>2</sub> ] <sub>n</sub>	30
2.7.5 Synthesis of Cu(3,5-lutidine) <sub>4</sub> SiF <sub>6</sub>	31
2.7.6 Synthesis of [Cu(pyrazine) <sub>2</sub> (SiF <sub>6</sub> )(H <sub>2</sub> O)] <sub>n</sub>	31
2.7.7 Synthesis of [Cu(pyrazine) <sub>2</sub> SiF <sub>6</sub> ] <sub>n</sub>	31
<b>2.8 Conclusions</b>	31
<b>References</b>	32
<b>Tables and Figures</b>	
<b>Tables</b>	
Table 1.1 Relative Dissociation Energies of Several Intermolecular Interactions	3
Table 2.1 Calculated Bond Distances for Synthesized MOMs	26
<b>Figures</b>	
Figure 1.1: Metal-Organic Materials contain a range of dimensional structures.	5
Figure 1.2: The 4,4'-bipyrdyl ditopic linker	7

Figure 1.3: $[\text{Zn}(4,4'\text{-bipyridine})_2(\text{H}_2\text{O})_2\cdot\text{SiF}_6]_n$	7
Figure 1.4: Pictorial representation of pillared square grids	8
Figure 1.5: $[\text{Zn}(4,4'\text{-bi}2\text{-pyridyl})_2(\text{SiF}_6)]_n$	8
Figure 1.6: $[\text{Cu}(4,4'\text{-bipyridine})_2\text{SiF}_6]_n$	9
Figure 2.1: Three pyridine based organic linkers to synthesize isorecticular MOMs.	10
Figure 2.2: XRPD for $[\text{Cu}(4,4'\text{-bipyridine})_2\text{SiF}_6]_n$ calculated and experimental	11
Figure 2.3: TGA of $[\text{Cu}(4,4'\text{-bipyridine})_2\text{SiF}_6]_n$	12
Figure 2.4: 2D $\rightarrow$ 3D polycatenated $\{[\text{Cu}(1,2\text{-Di}(4\text{-pyridyl)ethylene})_2(\text{H}_2\text{O})_2](\text{SiF}_6)(\text{H}_2\text{O})\}_n$	13
Figure 2.5: IR for ion exchange of $\text{Cl}^-$ for $\text{SiF}_6^-$ in 2D $\rightarrow$ 3D polycatenated structure	14
Figure 2.6: XRPD after $\text{Cl}^-$ ion exchange	14
Figure 2.7: Structure of $[\text{Cu}(1,2\text{-Di}(4\text{-pyridyl)ethylene})_2\text{SiF}_6]_n$ with pore diameter 13.3 Å.	16
Figure 2.8: XRPD of calculated v. theoretical for $[\text{Cu}(1,2\text{-Di}(4\text{-pyridyl)ethylene})_2\text{SiF}_6]_n$ .	17
Figure 2.9: TGA of $[\text{Cu}(1,2\text{-Di}(4\text{-pyridyl)ethylene})_2\text{SiF}_6]_n$ .	17
Figure 2.10: $[\text{Cu}(\text{pyrazine})(\text{SiF}_6)(\text{H}_2\text{O})_2]$	18
Figure 2.11: $\text{Cu}(3,5\text{-lutidine})_4$	19
Figure 2.12: $\text{Cu}(\text{pyrazine})_2(\text{SiF}_6)(\text{H}_2\text{O})$	20
Figure 2.13: XRPD $\text{Cu}(\text{pyrazine})_2(\text{SiF}_6)(\text{H}_2\text{O})$ vs. calculated $[\text{Cu}(\text{pyrazine})_2\text{SiF}_6]_n$ .	21
Figure 2.14: Structure of $[\text{Cu}(\text{pyrazine})_2\text{SiF}_6]_n$ with pore diameter 6.85 Å.	22
Figure 2.15: XRPD of calculated and experimental $[\text{Cu}(\text{pyrazine})_2\text{SiF}_6]_n$ .	22
Figure 2.16: TGA for $[\text{Cu}(\text{pyrazine})_2\text{SiF}_6]_n$	23
Figure 2.17: Three isorecticular MOMs	24
Figure 2.18: TGA for $[\text{Cu}(\text{pyrazine})_2\text{SiF}_6]_n$ , $[\text{Cu}(4,4\text{-bipyridyl})_2\text{SiF}_6]_n$ , and $[\text{Cu}(1,2\text{-Di}(4\text{-pyridyl)ethylene})_2\text{SiF}_6]_n$ .	25
Figure 2.19: B.E.T. surface area for $[\text{Cu}(4,4'\text{-bipyridyl})_2\text{SiF}_6]_n$ and $[\text{Cu}(1,2\text{-Di}(4\text{-pyridyl)ethylene})_2\text{SiF}_6]_n$	27

# Chapter 1

## Introduction

### 1.1 Preamble

*“... I can hardly doubt that when we have some control of the arrangement of things on a small scale we will get an enormously greater range of possible properties that substances can have, and of different things that we can do.”*

Richard P. Feynman<sup>1</sup>

*“One of the continuing scandals in the physical sciences is that it remains in general impossible to predict the structure of even the simplest crystalline solids from a knowledge of their chemical composition.”*

John Maddox<sup>2</sup>

The human mind has always desired the ability to predict forthcoming events. For millennia people have tried to make accurate predictions. From natural disasters to the end of the human race, there has been an enticing aurora around the idea of prediction. However, it is generally impossible to predict something without first understanding the concept of how and why it occurs. All fields of science have felt the effects of this predicament. Scientists try to grasp the evidence presented to them and make accurate predictions about the how something will work, but without the correct knowledge, many predictions fail. However, gaining knowledge through observation and experimentation helps scientists to understand inner workings, its form. This form leads to a function. Understanding this function can then lead to the ability to accurately predict experimental and physical outcomes.

Feynman understood that knowing and controlling structural outcomes will lead to vast, new properties and an array of ways scientists can manipulate forms to create highly specific functions. However, as stated by Maddox, it is still very difficult to make predictions of simple crystal structures without being able to control how and why certain chemical frameworks occur. The scientific fields of supramolecular chemistry and crystal engineering are now trying take on this difficult task to make new materials for real world applications.

## 1.2 Supramolecular Chemistry

*“Supramolecular chemistry is a highly interdisciplinary field of science covering the chemical, physical, and biological features of the chemical species of greater complexity than molecules themselves, that are held together and organized by means of intermolecular (non-covalent) binding interactions.”*

*“chemistry beyond the molecule”*

Jean-Marie Lehn<sup>3,4</sup>

### 1.2.1 Supramolecular History

To understand the functions of materials in the physical world we occupy, we must first understand how these materials assemble as form equals function. Intermolecular forces, first postulated by Johannes Diderik van der Waals in 1873, are noncovalent interactions between molecules. Supramolecular chemistry, or simply put ‘chemistry beyond the molecule’, is primarily governed by these intermolecular, noncovalent interactions. Noncovalent interactions came to light in 1894 with Fischer’s lock and key principle to explain the substrate-enzyme complex and molecular recognition.<sup>5</sup> Similarly, the Alfred Werner introduction into coordination chemistry through a differentiation between coordinated and ionic species using cobalt ions laid the foundation for modern inorganic chemistry.<sup>6</sup> In 1949, the “Ubermolecules” or “Supermolecules” found by Wolf and Wolffe<sup>7</sup> were later described and explained by hydrogen bonding and self-assembly when Pauling published his most significant scientific contribution in “The Nature of the Chemical Bond” .<sup>8</sup> Watson and Crick continued the growing interest in noncovalent chemistry by using crystallography to determine hydrogen bonding between DNA base pairing and ultimately leading to its double helical structure.<sup>9</sup>

### 1.2.2 The Noncovalent Bond

In the supramolecular world, noncovalent interactions dominate. Theoretical calculations with quantum mechanics have yielded a series of known intermolecular interactions that govern supramolecular chemistry. **Table 1.1** shows relative dissociation energies of the different interactions seen in this branch of chemistry.

**Table 1.1 Relative Dissociation Energies**

Interaction	Dissociation Energy (kJ/mol)	Example Compounds
London Dispersion, van der Waals	1 - 10 kJ/mol	Inert gases
Dipole-dipole	3 - 4 kJ/mol	HCl
Ion-dipole, coordinate covalent	5 - 50 kJ/mol	Coordination complexes M-L
Hydrogen bonding	5 - 40 kJ/mol	Co-crystals, carboxylic acid dimer
$\pi$ - $\pi$ , CH- $\pi$	1 - 50 kJ/mol	Benzene
Covalent	100 - 1000 kJ/mol	C-C, C=C
Ionic	100 - 1000 kJ/mol	K <sup>+</sup> Cl <sup>-</sup>

The coordinate covalent bond, as found in metal-organics, is a reversible bond between shared electrons of a metal ion and a non-carbon atom of significantly lower strength than a covalent bond. Coordinate covalent systems assemble under mild conditions and allow for the spontaneous assembly of ordered structures. Their lower dissociation energies allow for reversibility which promotes self correction not found in covalently and ionic compounds. Hydrogen bonding, the most significant of all intermolecular interactions, is the attractive interaction of a hydrogen atom with an electronegative atom which possesses a lone pair such as oxygen and nitrogen. The hydrogen bond is primarily responsible for life sustaining interactions between the base pairs of nucleic acids found in DNA.<sup>9</sup>

### 1.3 Crystal Engineering

*“...crystal engineering, which is defined as the understanding of intermolecular interactions in the context of crystal packing and in the utilisation [sic] of such understanding in the design of new solids with desired physical and chemical properties...The almost perfect alignment of molecules in an organic crystal results usually in highly predictable physical and chemical properties which in turn justify efforts at crystal engineering.”*

Guatum R. Desiraju<sup>10</sup>

### ***1.3.1 History of Crystal Engineering***

Crystal engineering aims to design solid-state materials by prediction of reactants to yield a desired product. Product predictions will allow for specific properties to be tailored for future needs in energy application with gas storage, catalysis, and environmental issues to sequester toxic chemicals from the environment. Being able to predict crystal structure will bring to light Feynman's<sup>1</sup> vision for vastly new materials with specific applications. Ever increasing efforts in increasing resolution and analytical techniques has continued to propel crystal engineering to the field it is today.

Desiraju, a pioneer in crystal engineering, along with scientists like Etter<sup>11</sup> helped advance the field by describing noncovalent intermolecular interactions with small organic molecules.<sup>10,12,13</sup> Investigations such as these along with crystal databases like the Cambridge Structural Database (CSD) have helped increase prediction capabilities.

## **1.4 Metal-Organic Materials**

### ***1.4.1 Introduction to the Metal-Organic Material***

Over the past two decades there has been a tremendous push to develop nano-materials for applications in everyday life. Metal-Organic Materials, MOMs, are now at the forefront of this scientific endeavor as the world pushes for clean energy sources and “green” chemistry. MOMs consist of the coordination of an organic linker with a metal node to create network topologies that mimic zeolites for specific applications through a process of self-assembly. The coordination bond as shown in **Table 1.1** has a much weaker interaction than ionic or covalent bonding promoting reversibility and self-correction. Self-assembly and reversibility give MOMs the ability to be tailored to fit specific needs and crystal engineered to develop specific properties. MOMs are extremely malleable to varying conditions thus providing many different crystalline

products despite using identical reagents. These materials form structures of differing dimensionality as shown in **Figure 1.1**.

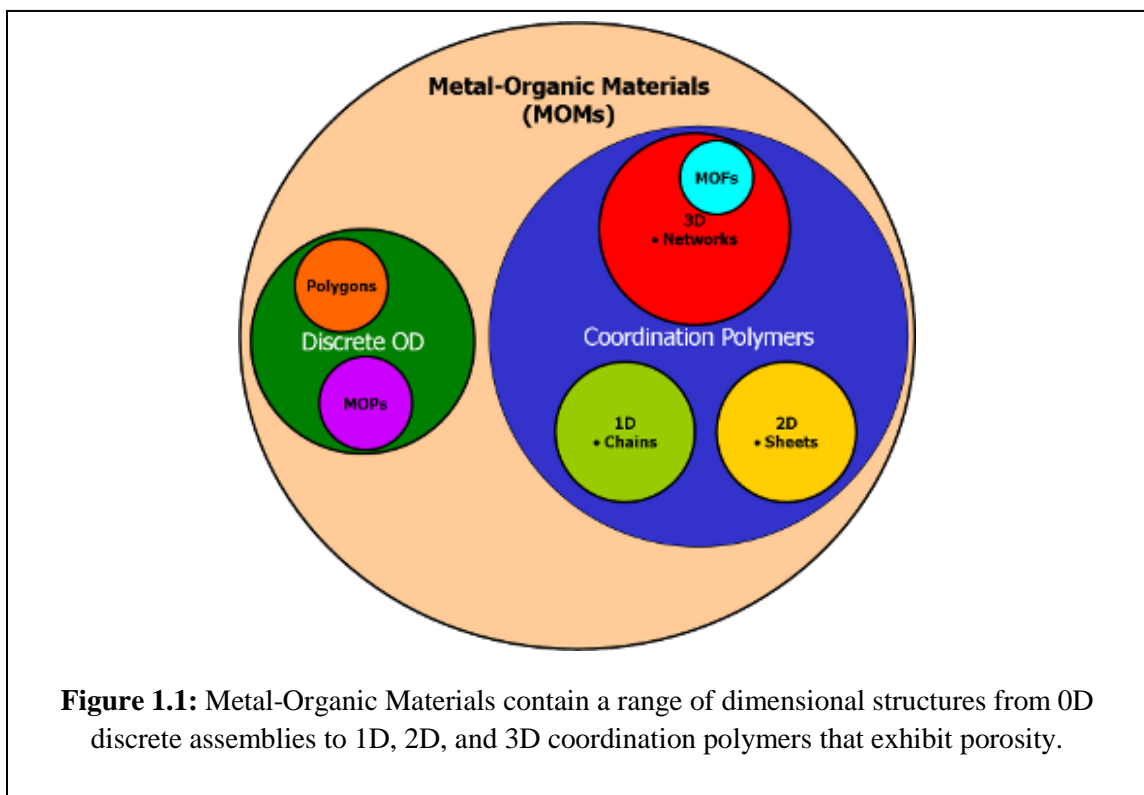


**Figure 1.1:** Metal-Organic Materials contain a range of dimensional structures from 0D discrete assemblies to 1D, 2D, and 3D coordination polymers that exhibit porosity.

#### ***1.4.2 History of the MOM***

Metal-Organic Materials is a young branch of inorganic chemistry, not having been fully realized until the late 1980s and early 1990s. Coordination chemistry, as stated previously, began with Werner<sup>6</sup> in 1893, but the first metal-organic frameworks, MOFs, came out nearly a century later. The field has since forth attracted vast attention because of the wide array of previously mentioned properties of gas storage, gas sequestration, and catalysis. These crystalline materials are constructed using metal nodes and organic linkers to produce new structures with unrivaled surface area and permanent surface area. The linkers act as spacers to link metal centers in which large, empty structures evolve. Work done by Robson in the early 1990s used metal nodes and organic linkers to form diamond-like networks and interpenetrated square grids, some of the first

metal-organic frameworks (MOFs).<sup>14,15</sup> Work done by Kitagawa<sup>16-18</sup>, Fujita<sup>19-23</sup>, Robl<sup>24,25</sup>, Zaworotko<sup>26-28</sup>, Hosseini<sup>29,30</sup>, and others<sup>31,32</sup> have helped advance metal-organics into the most anticipated and exciting fields of coordination chemistry.

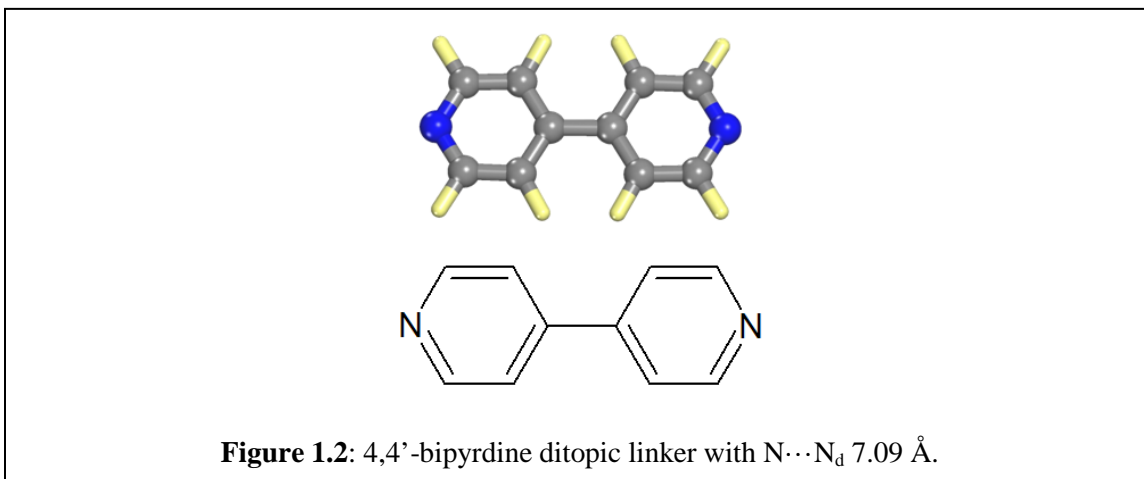
With the explosion of interest in metal-organics during the early 1990s a series of acronyms were adopted to characterize and classify these new compounds. Porous Coordination Polymers (PCPs), Metal-Organic Frameworks (MOFs), Materials Institute Lavoisier (MILs), and University of Michigan Crystalline Materials (UMCMs) became the more widely used acronyms. These new materials went beyond previous metal-organics by employing metal clusters and a wide range of spacers in place of strictly ditopic linkers.<sup>31,32</sup> A.F. Wells used a new 'node and spacer' terminology to help classify these new compounds on a topological basis.<sup>33</sup> Metal-organics now take into account new Secondary Building Units (SBUs) and extended carboxylate and pyridine based links to form vastly porous structures typically from 1000-4000 m<sup>2</sup>/g and one has even reached 10,000 m<sup>2</sup>/g.<sup>34</sup> This vastly outcompetes any other previously synthesized porous materials such as zeolites. This porosity is useful in storing large amounts of gas in a small amount of compound, encapsulating porphyrins, performing catalysis, and uptaking guest molecules.

#### ***1.4.3 Properties of MOMs***

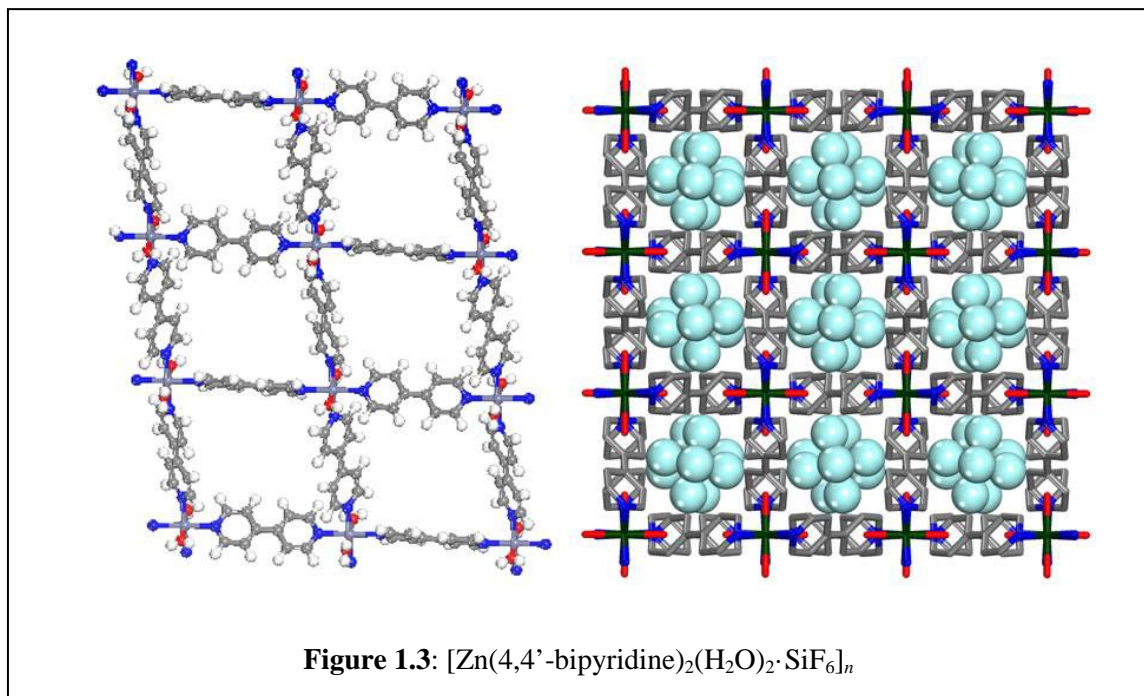
MOMs can be characterized based on functionality and application. Functional MOMs rely on porosity. Accessible pores and interactions with adsorbate (functionality) give each MOM unique properties that are modifiable to fit specific needs. Materials in metal-organics are known to be permanently porous with high surface area ranging from several hundred to several thousand m<sup>2</sup>/g.<sup>16,18,28</sup> Pore tuning also allows for new applications like molecule sequestration and selectivity, catalysis, and ion exchange. As crystal engineering advances, structural predictions will become more accurate, giving vastly more control of the properties of MOMs.

##### ***1.4.3.1 The 4,4'-bipyridyl linker and its impact***

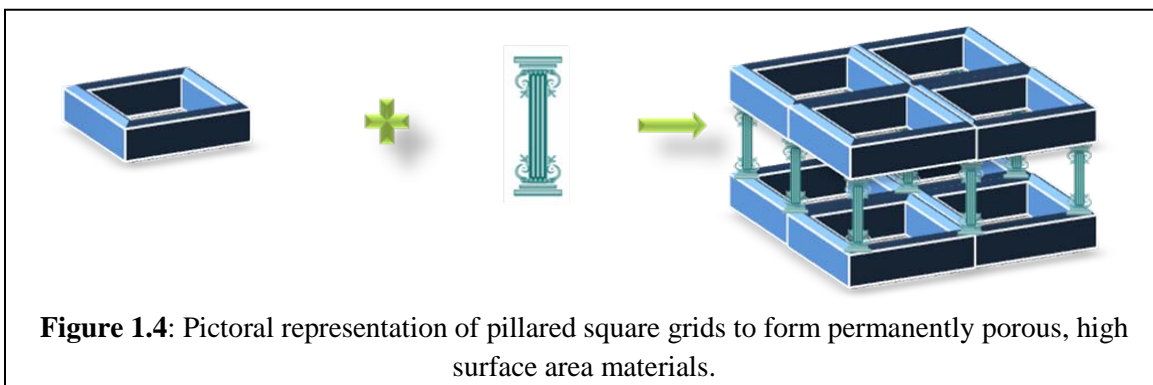
Of the first MOMs to be recognized was Robson's work with the 4,4' bipyridyl linker. This ditopic, linear organic linker, shown in **Figure 1.2**, has two nitrogen atoms forming coordination bonds with a metal center to form various structures that contain open space or free volume.



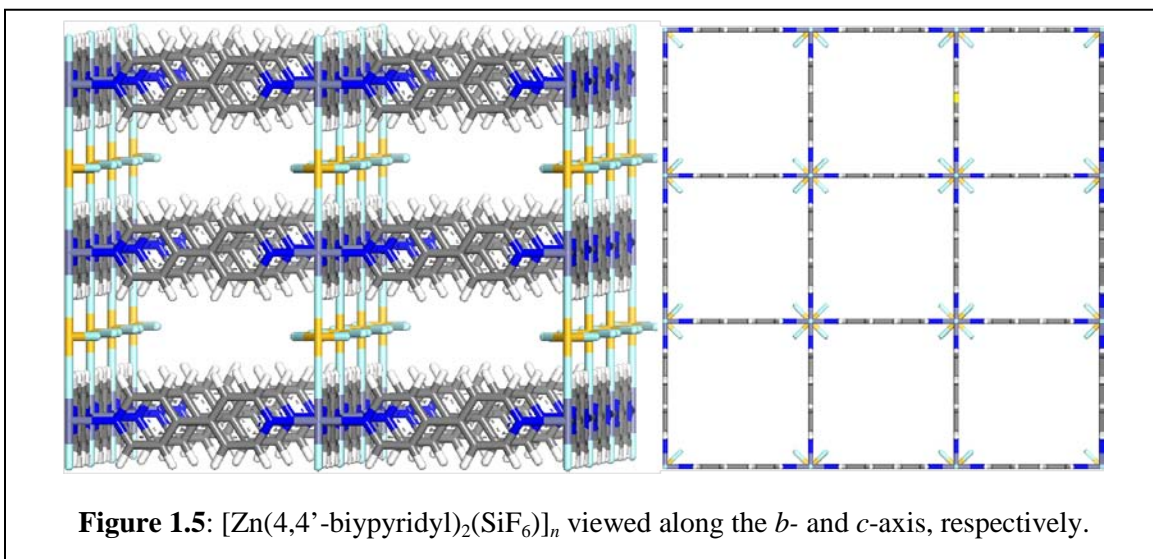
The interpenetrated framework using an octahedral zinc node created independent square grids with two water molecules coordinated in the axial positions with hexafluorosilicate (SiF<sub>6</sub>) as a counter ion as shown in **Figure 1.3**.<sup>14</sup>



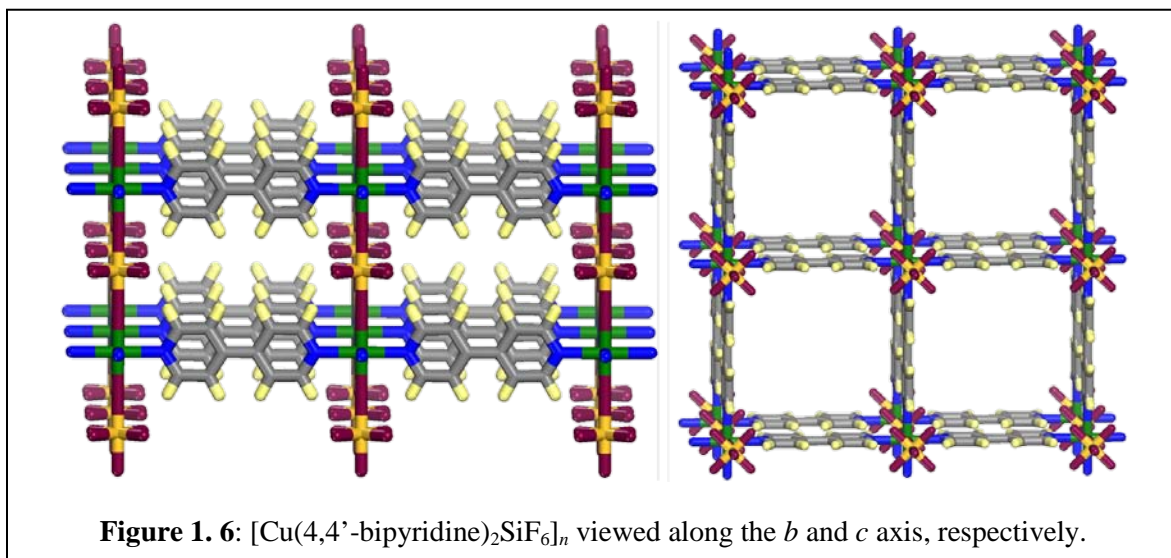
Interpenetration caused the MOM to be of low surface area and low porosity as the framework was filled with square grid sheets. Fujita in 1994, however, discovered new applications for interpenetrated 4,4'-bipyridyl frameworks such as catalysis and clathration. The cadmium (II) based structure showed clathration of *o*-dibromobenzene and the catalytic ability for cyanosilylation of aldehydes.<sup>35</sup> Work done by Zaworotko's group a year later built upon Robson's structure to form non-interpenetrated pillared square grid sheets with high surface area.<sup>28</sup> **Figure 1.4** is a animated representation of pillared square grids to form permanently porous, high surface area MOMs.



Zaworotko *et al* used  $\text{ZnSiF}_6$  and the 4,4'-bipyridyl linker in a nonaqueous environment to create the first pillared sheets with unidirectional pores. This pillared framework, represented in **Figure 1.5**, used  $\text{SiF}_6$  as a pillaring agent to make large pores running down the *c*-axis.



The structure shown in **Figure 1.5**, however, was not water stability and upon introduction to the atmosphere moisture caused loss of crystalline integrity and structural degradation. Kitagawa improved pillared MOMs by synthesizing a water stable porous MOM with surface area of 1300 m<sup>2</sup>/g using a copper node.<sup>18</sup> The structure used identical pillaring agent and linker as Zaworotko's Zn-MOM to form pillared square grids that are water stable and retain structural integrity with solvent evacuation. This new structure, represented in **Figure 1.6**, showed enormous methane adsorption as compared to its zeolite predecessors proving the massive storage capabilities of MOMs.



Now extended and shortened variants of the 4,4'-bipyridyl linker are being used to alter and design structures for selectivity of gas molecules.<sup>29</sup>

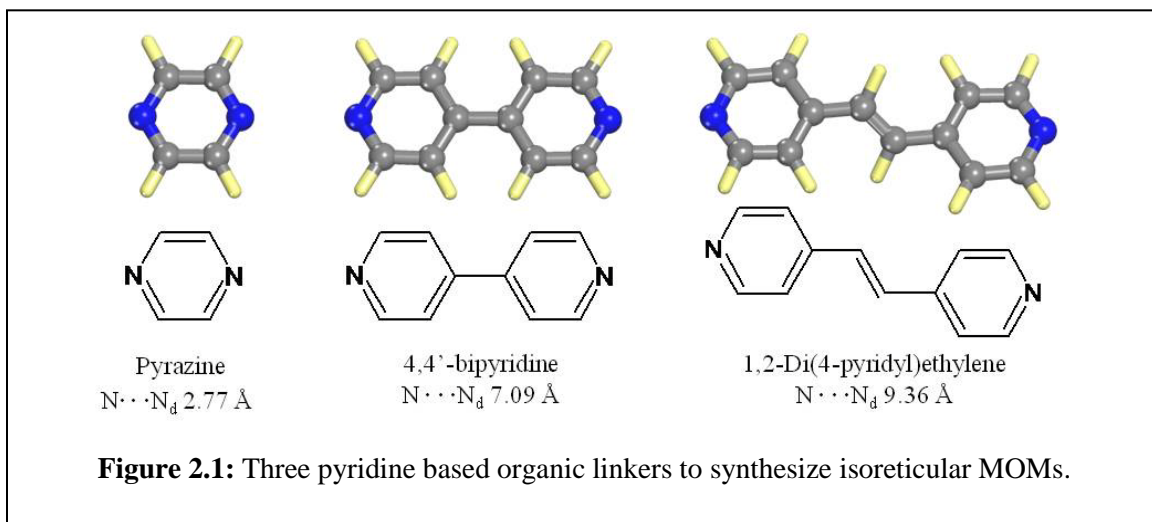
## Chapter 2

### Synthesis of Three Isorecticular MOMs

#### 2.1 Introduction

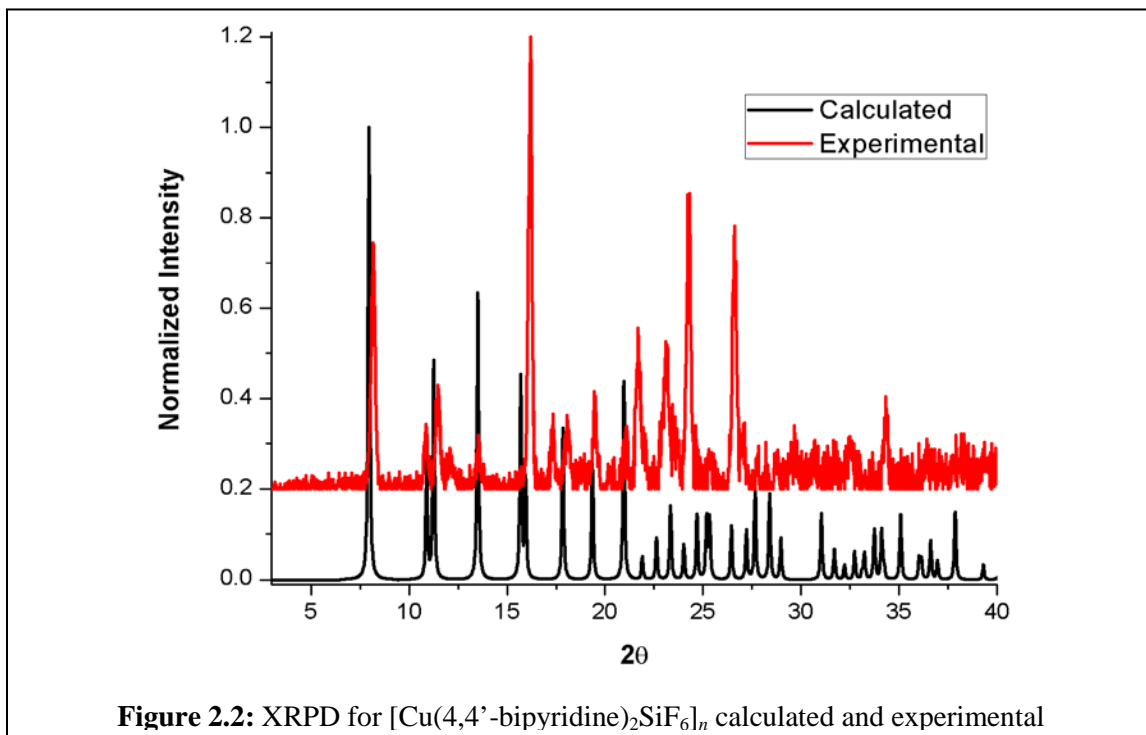
With the onset of crystal engineering and metal-organic materials, new crystalline materials specifically engineered for desired properties have been gaining vast attention. Accurate predictions of structures will allow for vastly more possibilities in application of new materials. Of some of the first MOMs to be synthesized, those using the 4,4'-bipyridine linker were of vital importance in helping to develop the field. With the work done by Robson<sup>14</sup>, Fujita<sup>35</sup> Zaworotko<sup>28</sup> and Kitagawa<sup>18</sup>, this particular linker transitioned from interpenetrated square grids to water stable pillared frameworks capable of unrivaled adsorption of gases.

New MOMs synthesized using several 4,4'-bipyridyl variants are desired in order to perform systematic evaluations of the affect of pore size on gas sorption and diffusion through the material. Shortened and extended pyridine based variants will allow for comparison studies of these properties. These linkers, pyrazine and 1,2-Di(4-pyridyl)ethylene, depicted in **Figure 2.1** are the analogues to be used. Using the copper node and hexafluorosilicate found in Kitagawa's structure, three isorecticular MOMs can be synthesized to perform the previously mentioned diffusion and sorption studies.

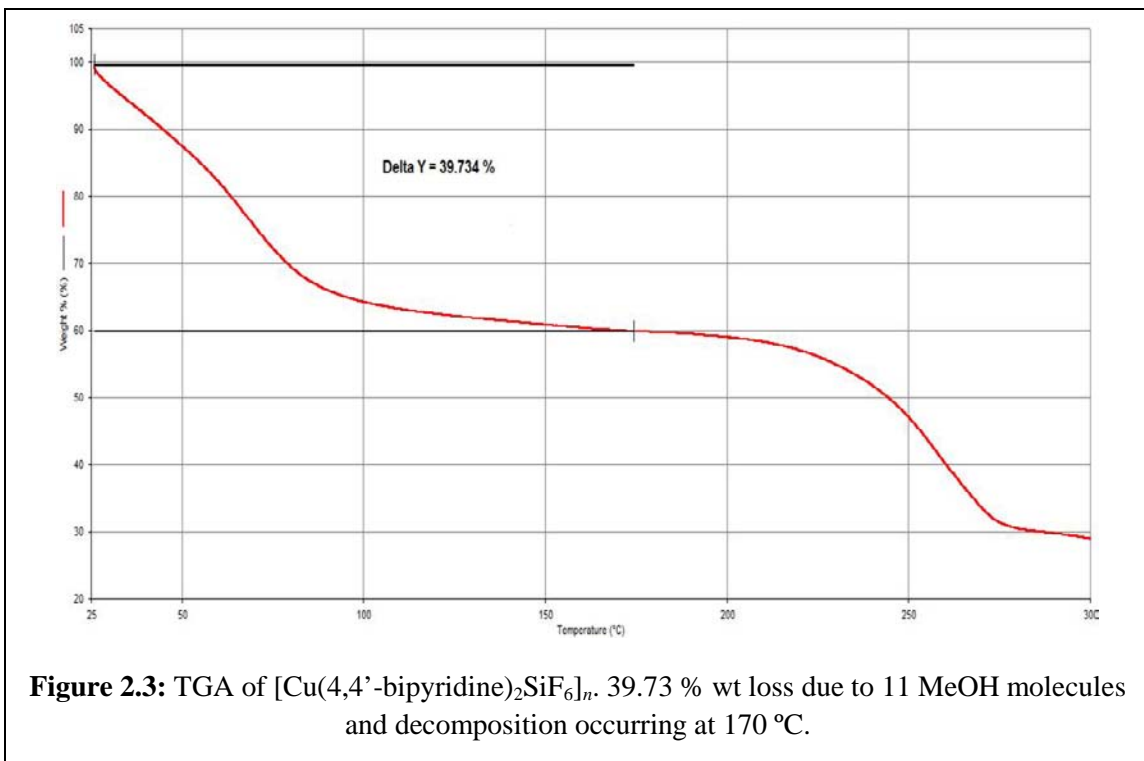


## 2.2 Synthesis of $[\text{Cu}(4,4'\text{-bipyridyl})_2\text{SiF}_6]_n$

A reproduction of the Kitagawa's water stable  $[\text{Cu}(4,4'\text{-bipyridine})_2\text{SiF}_6]_n$  was performed under modified literature methods. The purple precipitate exhibited the XRPD shown in **Figure 2.2** which is matched to a calculated XRPD for the structure. Methodologies are described in **Section 2.7**.



Thermal Gravimetric Analysis (TGA), **Figure 2.3**, of  $[\text{Cu}(4,4'\text{-bipyridine})_2\text{SiF}_6]_n$  shows an initial loss of approximately 11 MeOH molecules (39.73 % wt) from within the square channels of the framework. Decomposition begins at 170 °C after solvent loss.

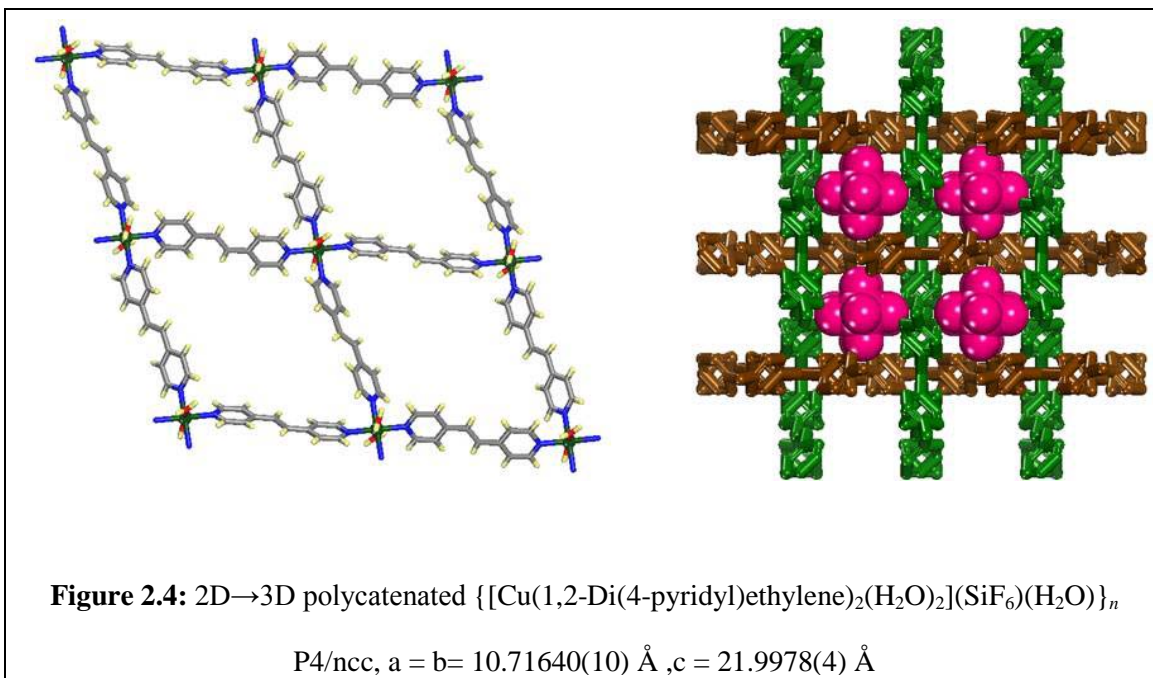


### 2.3 Synthesis of $[\text{Cu}(1,2\text{-Di}(4\text{-pyridyl)ethylene})_2\text{SiF}_6]_n$

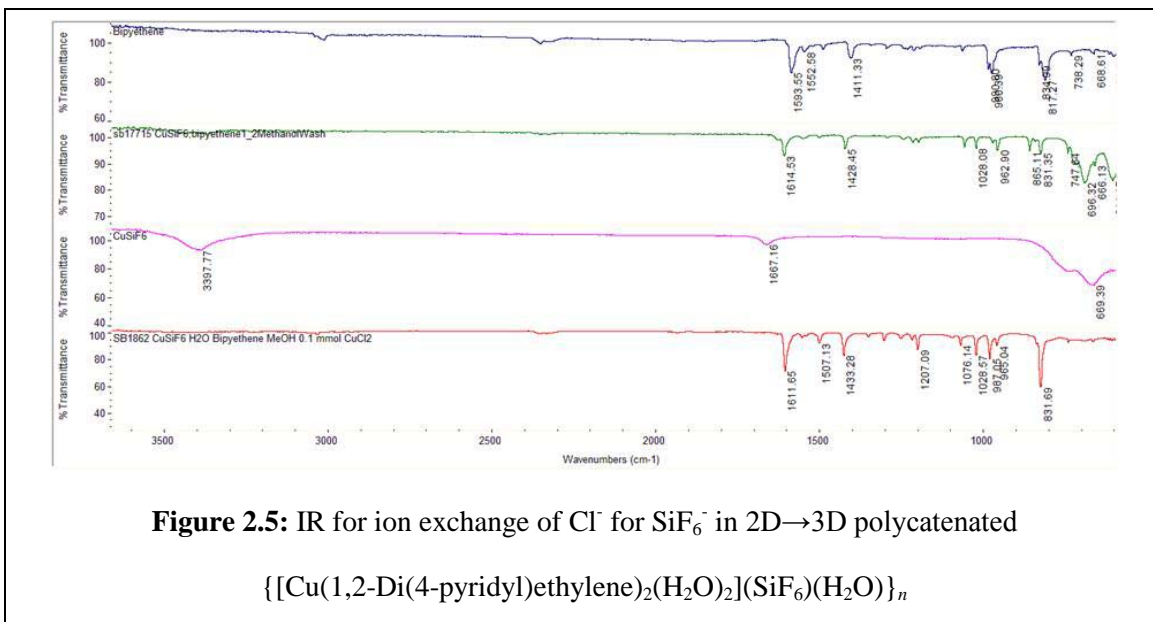
Synthesis of the extended analogue structure was attempted using a variety reactions altering solvent systems of  $\text{H}_2\text{O}$ , MeOH, DMSO, and DMF. Each of these systems was studied by varying temperature, concentration, and guest molecules to achieve the desired structure.

#### 2.3.1 $\{[\text{Cu}(1,2\text{-Di}(4\text{-pyridyl)ethylene})_2(\text{H}_2\text{O})_2](\text{SiF}_6)(\text{H}_2\text{O})\}_n$

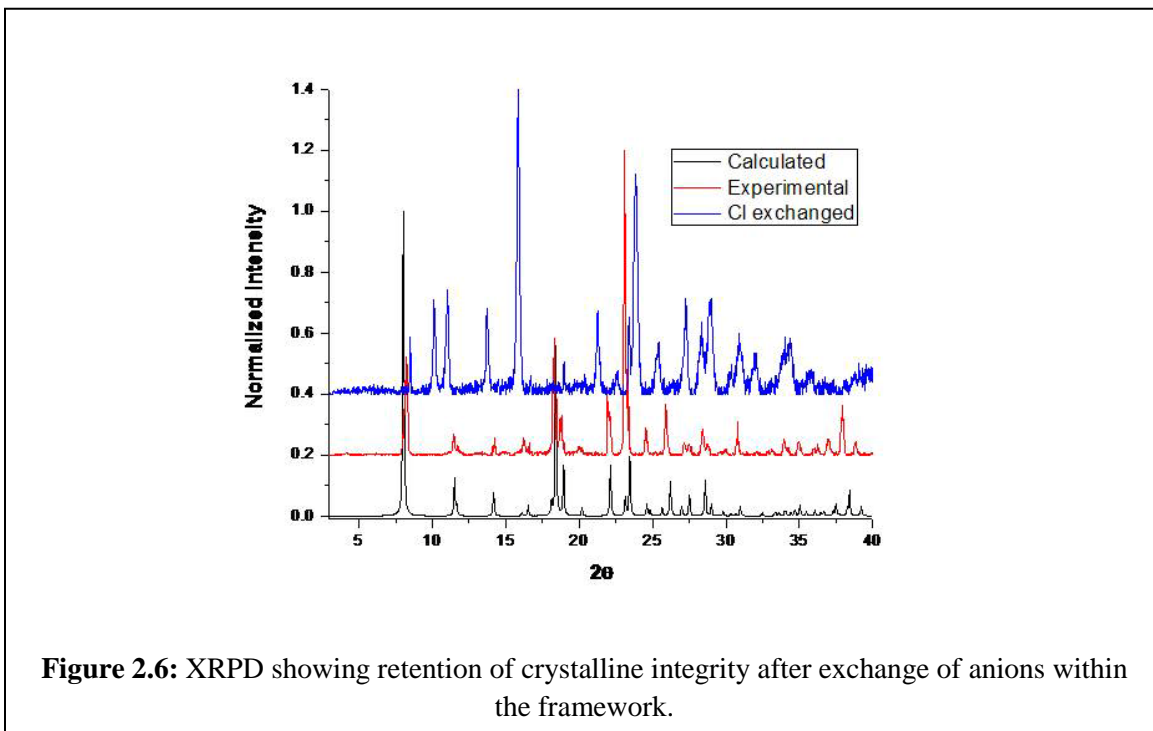
An intriguing 2D→3D polycatenated structure was synthesized through methodologies given in **Section 2.7**. The structure was characterized through Single Crystal X-Ray Diffraction. This polycatenated structure has two water molecules coordinated in the axial positions and forms entangled square grids as presented in **Figure 2.4**.



Due to the  $\text{SiF}_6^-$  anions inside the framework, ion exchange was studied to see if this structure can uptake chloride, phosphate, sulfate, and perchlorate. The first ion exchange was performed with  $\text{CuCl}_2$  to determine if small ions like chloride could be exchanged. **Figure 2.5** shows the IR of the starting materials, the original polycatenated structure with  $\text{SiF}_6^-$ , the exchanged framework, and  $\text{CuCl}_2$ . The loss of the  $\text{SiF}_6^-$  peak at  $696 \text{ cm}^{-1}$  with the chloride exchanged sample supports the loss of  $\text{SiF}_6^-$  and replacement by of  $\text{Cl}^-$ .



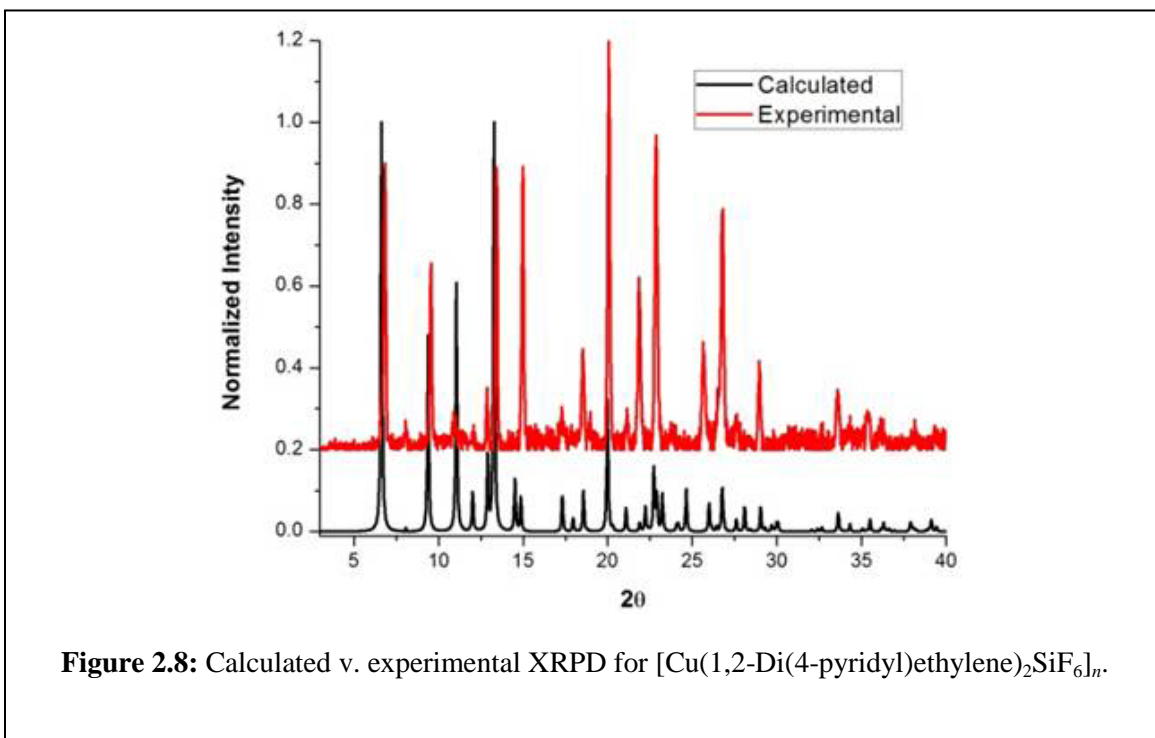
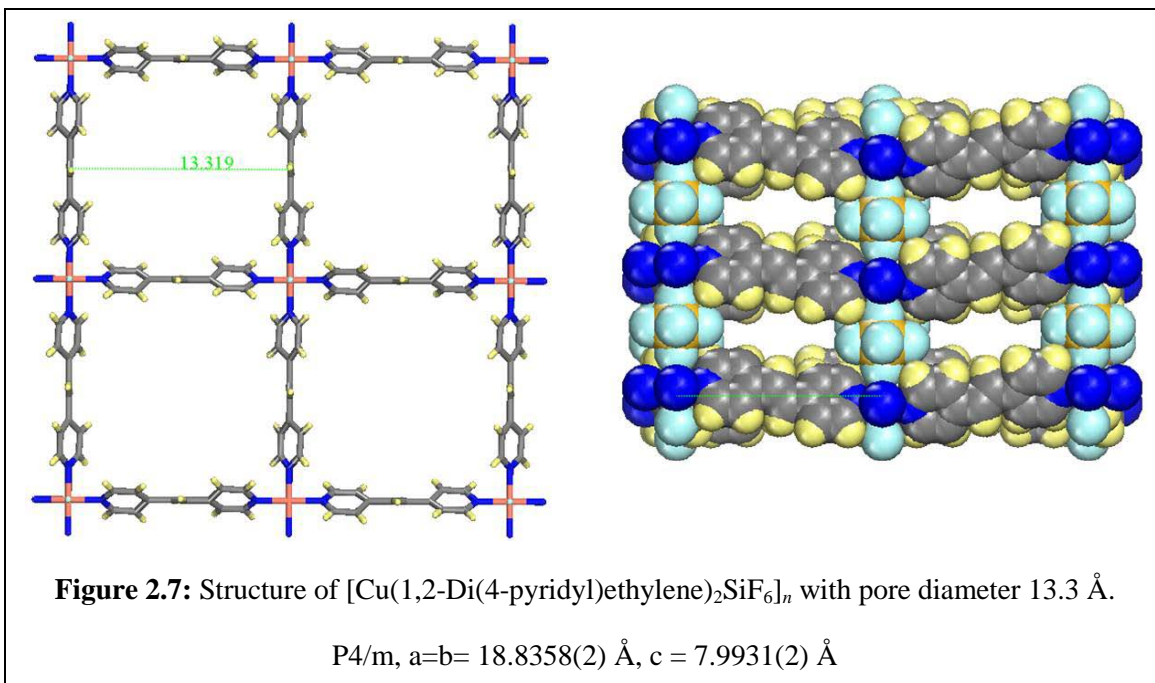
XRPD was measured to identify the polycatenated structure before and after ion exchange to determine if structural integrity remained intact. **Figure 2.6** shows XRPD data confirming the ability for the framework to uptake the chloride ion without decomposition of the framework.

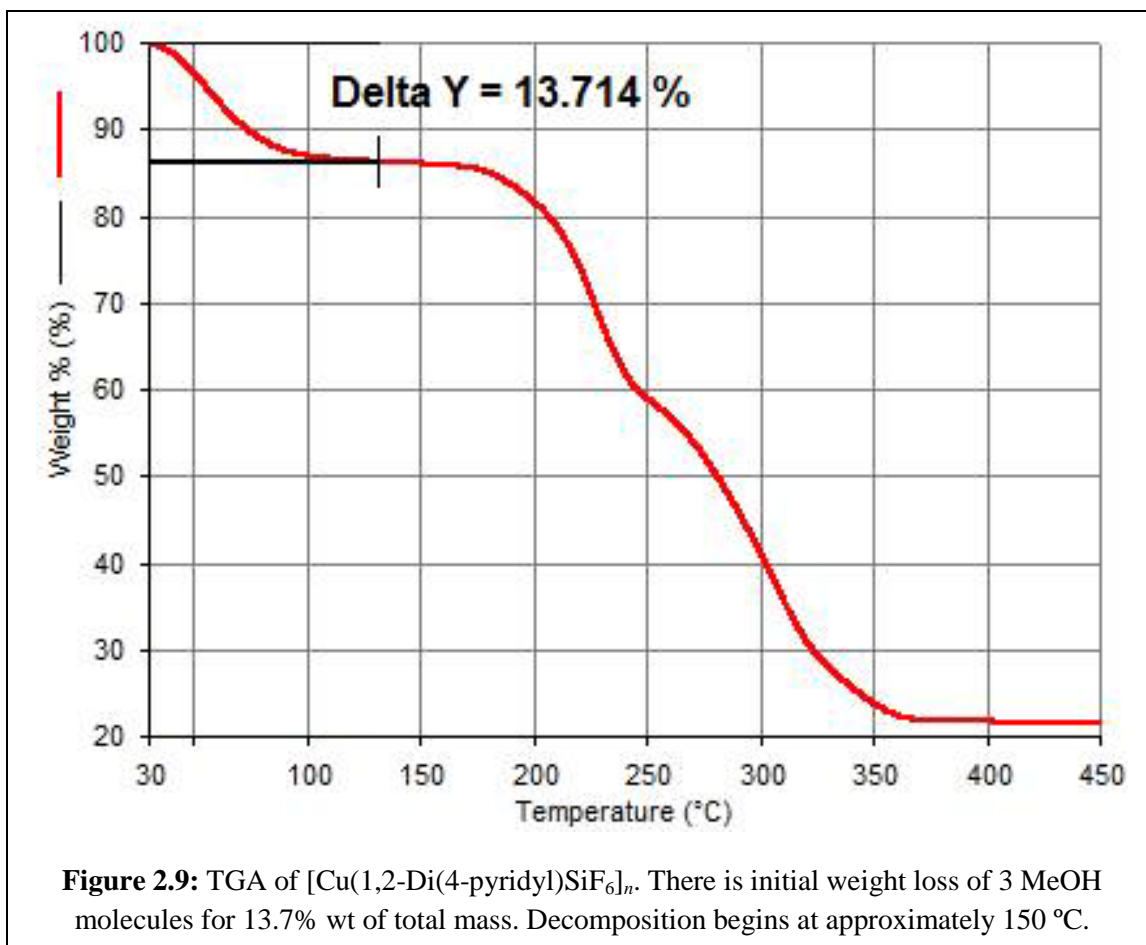


Later investigations were also undertaken to determine uptake of phosphate, sulfate, and perchlorate ions. However, IR showed no exchange for the sulfate or phosphate ion. Furthermore, the perchlorate ion caused decomposition of the framework as shown by XRPD. Additional experimentation will take place to determine if lower concentrations of the aforementioned ions can exchange into the framework.

### **2.3.2 [Cu(1,2-Di(4-pyridyl)ethylene)<sub>2</sub>SiF<sub>6</sub>]<sub>n</sub>**

After varying solvent conditions under solvothermal conditions did not yield the desired product, guest molecules 2,6-lutidine, 3,5-lutidine, and nitrobenzene were investigated. Single crystals were yielded with 2,6-lutidine guest and nitrobenzene guest. Single Crystal X-Ray Diffraction, XRPD, and TGA identified and characterized the structure represented in **Figure 2.7**, **Figure 2.8**, and **Figure 2.9**.



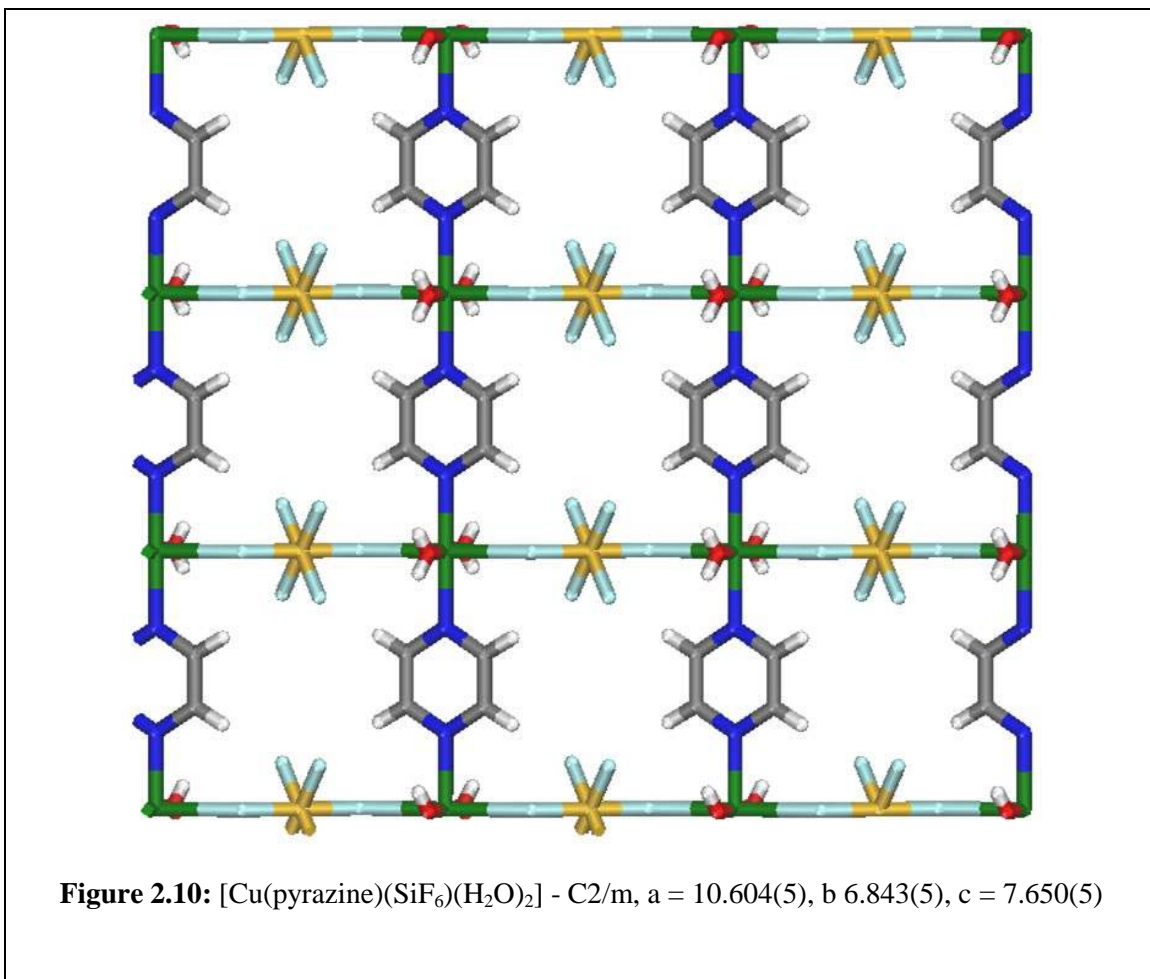


## 2.4 Synthesis of $[\text{Cu}(\text{pyrazine})_2\text{SiF}_6]_n$

Several different solvent systems of  $\text{H}_2\text{O}$ , MeOH, DMF, DMSO, and ethylene glycol were used under solvothermal and layered conditions to obtain the pyrazine structure. Also conditions such as temperature and concentrations were varied for each of these solvent systems. There were several interesting structures obtained in addition to the desired pillared  $[\text{Cu}(\text{pyrazine})_2\text{SiF}_6]_n$ .

### 2.4.1 $[\text{Cu}(\text{pyrazine})(\text{SiF}_6)(\text{H}_2\text{O})_2]$

The synthesized structure shown in **Figure 2.10** has two water molecules coordinated in the axial positions of the copper node. This water coordination caused the loss of two binding sites on the metal for the pyrazine ligand yielding square sheets.



#### 2.4.2 $\text{Cu}(\text{3,5-lutidine})_4\text{SiF}_6$

This structure was the product of using guest molecules to promote proper coordination around the metal center. Although this structure had the proper coordination, 3,5-lutidine outcompeted pyrazine for the equatorial coordination sites of the copper creating the long polymer chains represented in **Figure 2.11** instead of the desired square grids.

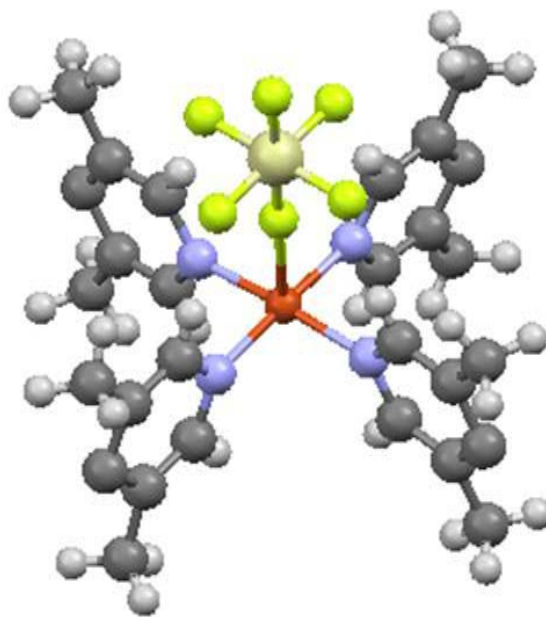


**Figure 2.11:**  $\text{Cu}(\text{3,5-lutidine})_4\text{SiF}_6$  - P4/n,  $a = 12.4958(19) \text{ \AA}$ ,  $c = 8.683(2) \text{ \AA}$

#### 2.4.3 $[\text{Cu}(\text{pyrazine})_2(\text{SiF}_6)(\text{H}_2\text{O})]_n$

This structure is slitted due to a very mild water coordination in the axial position as represented in **Figure 2.12**. The water molecule actually resides closer to the anionic  $\text{SiF}_6$  than the copper node. In order to try and remove the water molecule from the framework, heating was applied but the compound burnt due to excessive heating. XRPD, **Figure 2.13**, identified the compound as nearly matching the calculated pillared framework, but additional peaks show that it is not the desired product.

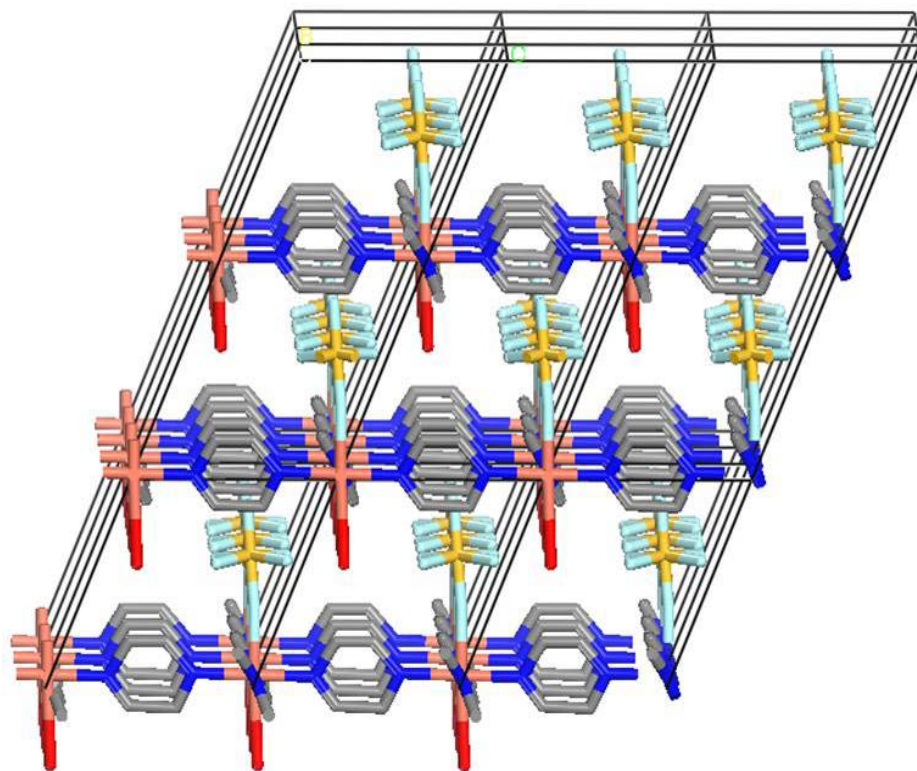
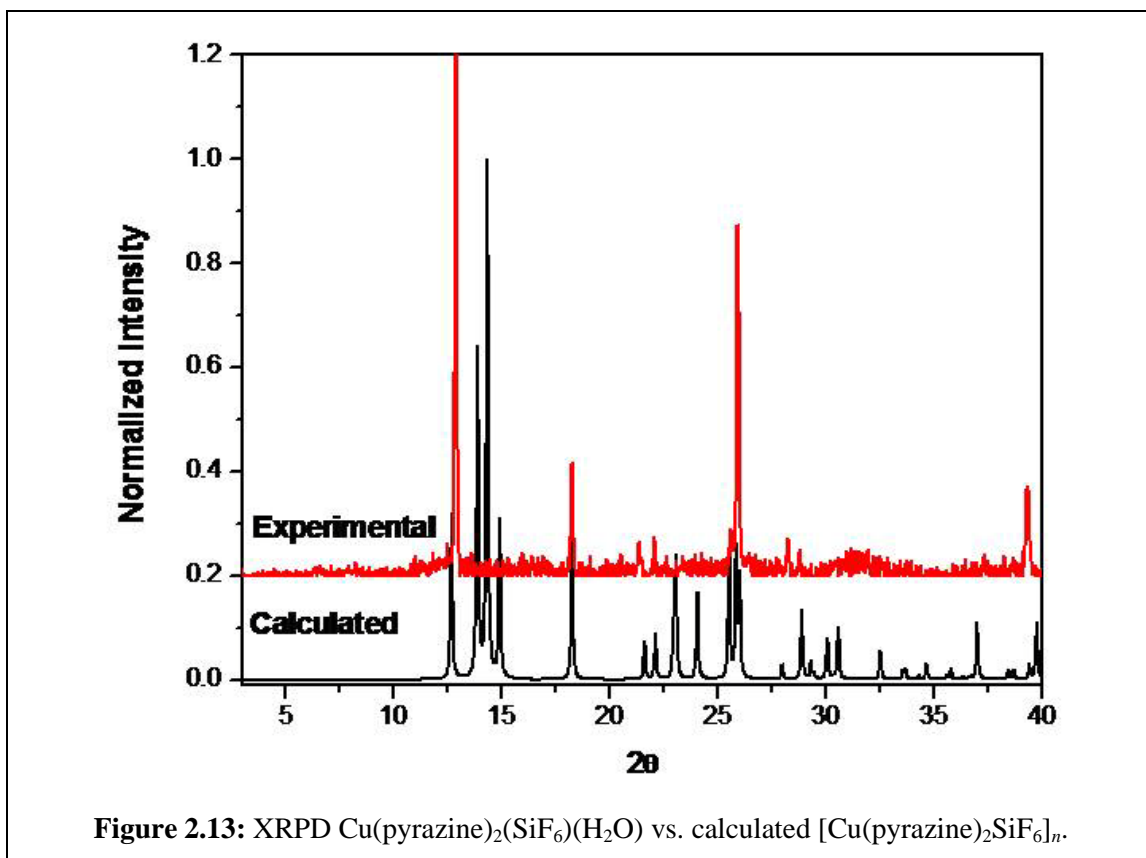


**Figure 2.12:**  $\text{Cu}(\text{pyrazine})_2(\text{SiF}_6)(\text{H}_2\text{O})$  -  $a = 15.033(3) \text{ \AA}$ ,  $b = 6.885(2) \text{ \AA}$ ,  $c = 6.868(2) \text{ \AA}$ ,  $\beta = 111.958(9)^\circ$



#### 2.4.4 $[\text{Cu}(\text{pyrazine})_2\text{SiF}_6]_n$

The desired crystal structure was obtained under anhydrous conditions. No single crystal was yielded however. The theoretical crystal structure shown in **Figure 2.14** was characterized with XRPD, **Figure 2.15**, to show that the product is the desired pillared framework. TGA was also performed and represented in **Figure 2. 16**.

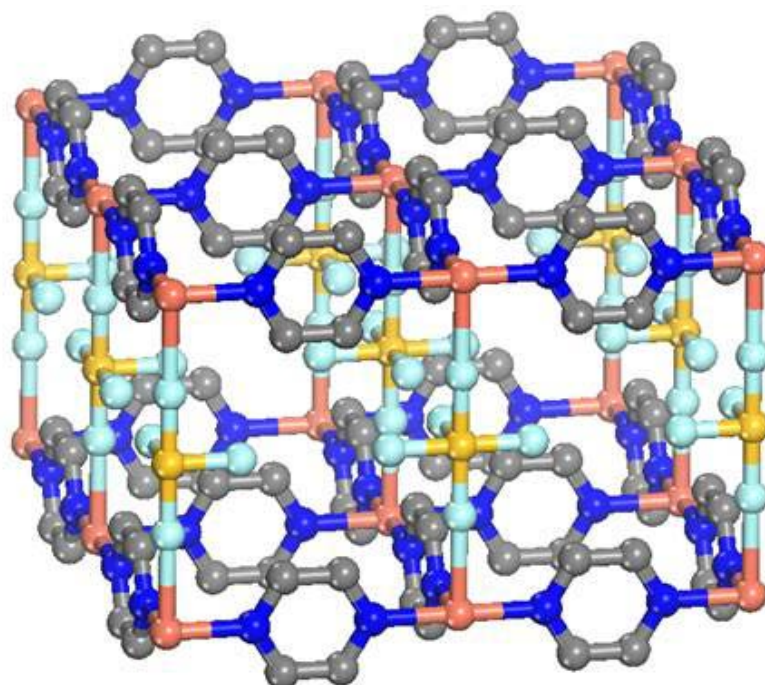


**Figure 2.14:**  $[\text{Cu}(\text{pyrazine})_2\text{SiF}_6]_n$  - P4/m,  $a = 6.8520 \text{ \AA}$ ,  $c = 8.1110 \text{ \AA}$ , windows  $6.85 \text{ \AA}$

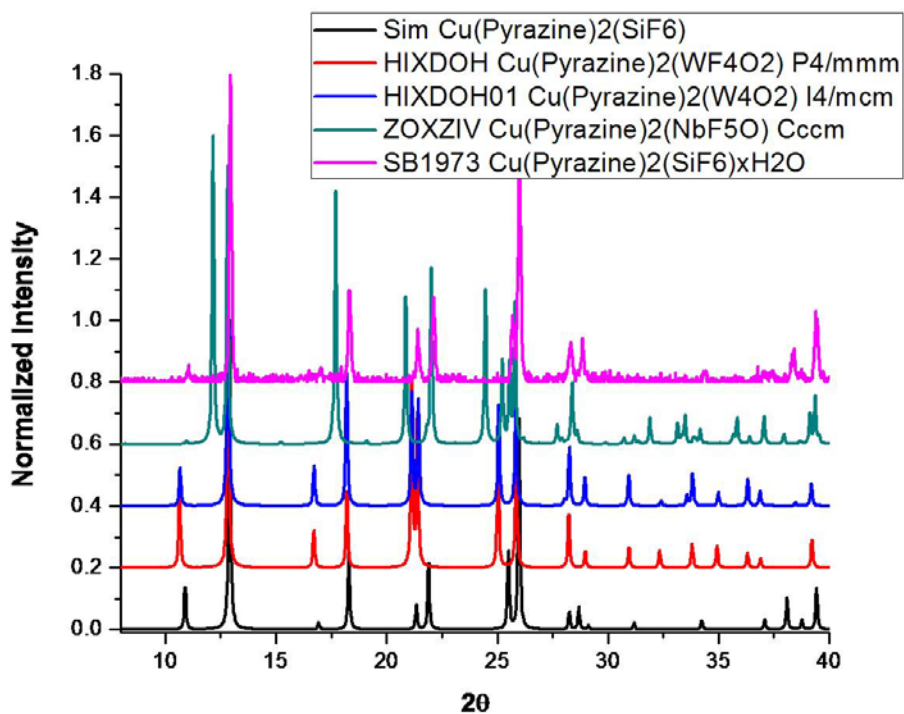


**Figure 2.15:** XRPD of calculated and experimental powder patterns for several pillared pyrazine structures including  $[\text{Cu}(\text{pyrazine})_2\text{SiF}_6]_n$ .

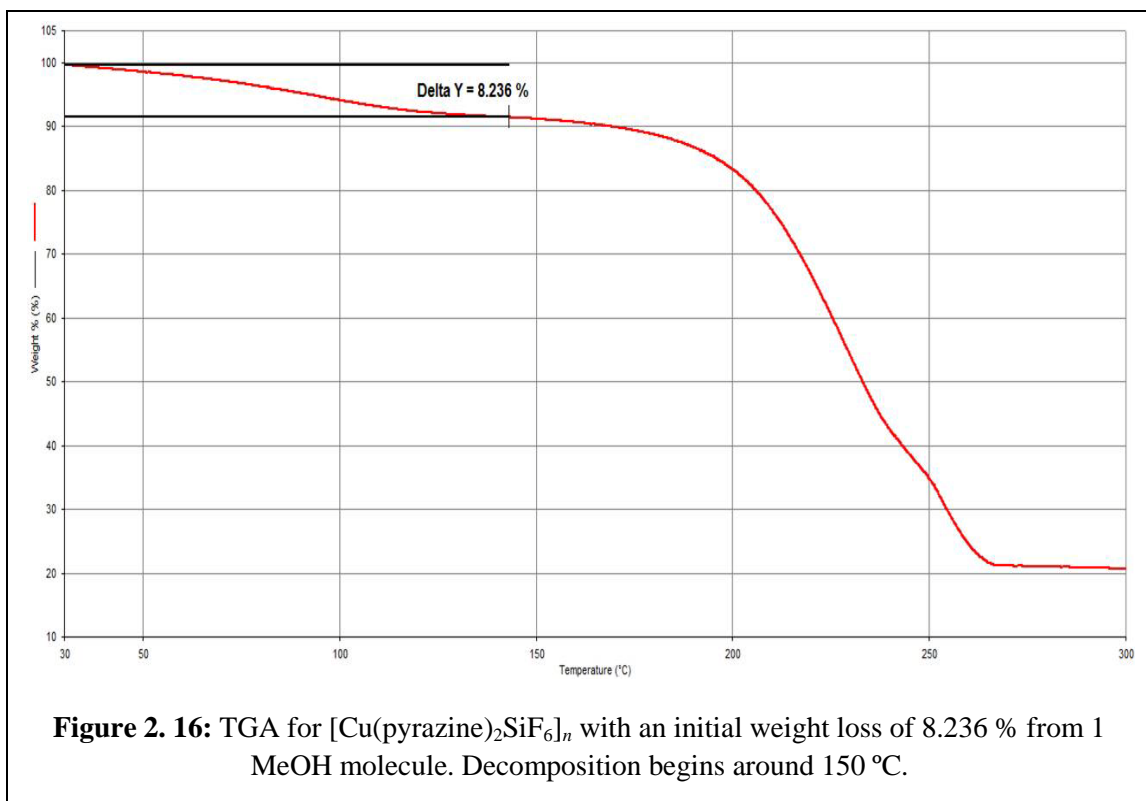
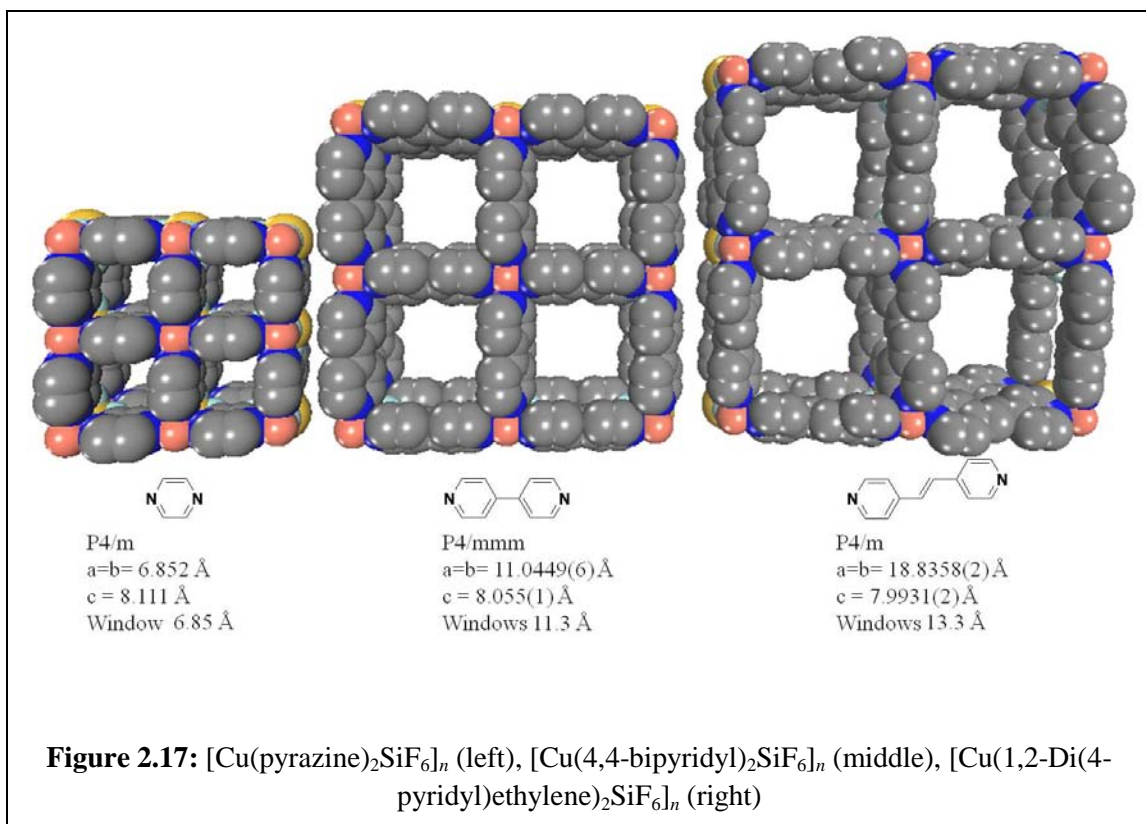


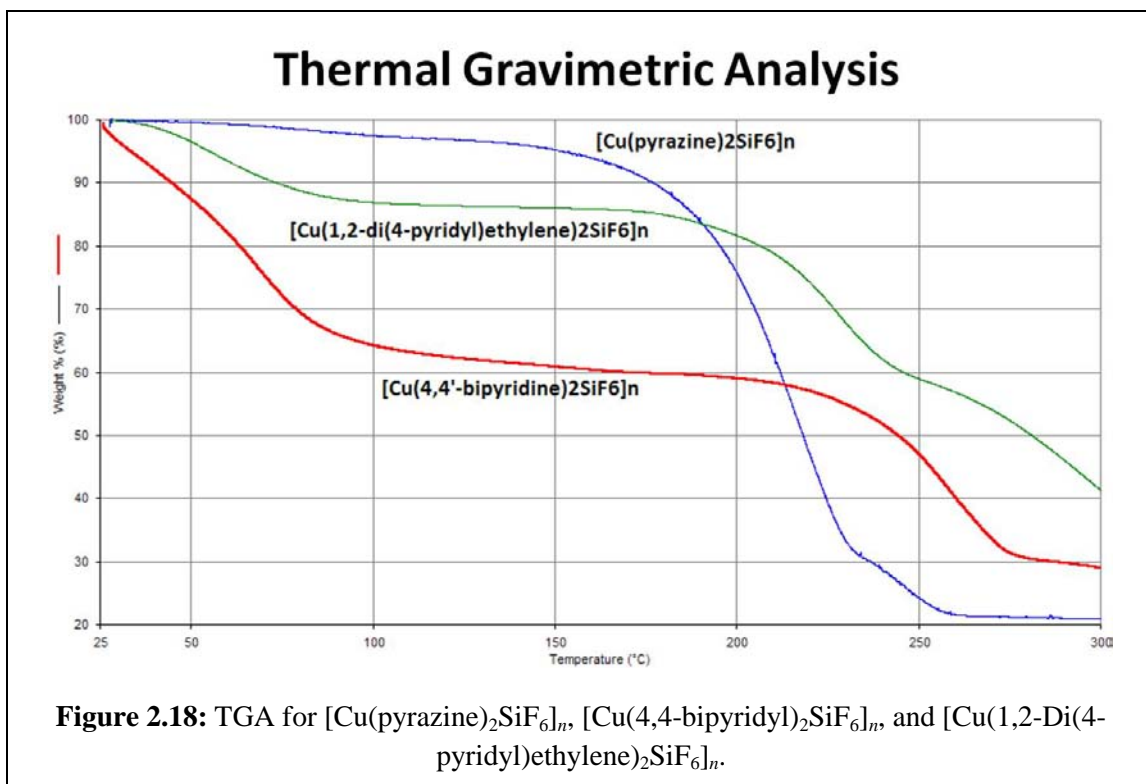
**Figure 2.17** is a visual representation of the framework size difference for the three synthesized pillared MOMs. Varying pore size will allow for systematic evaluations of gas sorption and diffusion properties.



## 2.5 Properties of Synthesized MOMs

### 2.5.1 Thermal Gravimetric Analysis

Thermal Gravimetric Analysis (TGA) aids in determining the thermal stability of materials. It measures a change in mass with an increase in temperature. TGA for the three synthesized isorecticular MOMs is represented in **Figure 2.18**. All TGAs were performed on a Perkin-Elmer STA 6000 Simultaneous Thermal Analyzer.



All three MOMs showed decent thermal stability with each beginning decomposition at greater than 150 °C. The initial weight loss shown in  $[\text{Cu}(4,4\text{'-bipyridine})_2\text{SiF}_6]_n$  and  $[\text{Cu}(1,2\text{-Di}(4\text{-pyridyl)ethylene})_2\text{SiF}_6]_n$  is from solvent evaporation within the framework.  $[\text{Cu}(1,2\text{-Di}(4\text{-pyridyl)ethylene})_2\text{SiF}_6]_n$  loses 3 MeOH molecules upon heating. Mass stabilization at around 100 °C shows complete loss of solvent and structural integrity is lost at 150 °C.  $[\text{Cu}(4,4\text{'-bipyridine})_2\text{SiF}_6]_n$  loses approximately 11 MeOH molecules until decomposition 170 °C.  $[\text{Cu}(\text{pyrazine})_2\text{SiF}_6]_n$  showed a small initial weight loss due to 1 MeOH molecule until decomposition began at 150 °C.

### 2.5.2 Bond Distances and Window Size

Each synthesized MOM,  $[\text{Cu}(\text{pyrazine})_2\text{SiF}_6]_n$  [1],  $[\text{Cu}(4,4\text{'-bipyridine})_2\text{SiF}_6]_n$  [2], and  $[\text{Cu}(1,2\text{-Di}(4\text{-pyridyl)ethylene})_2\text{SiF}_6]_n$  [3], were measured through crystal data and Mercury software for bond distances of  $\text{Cu}\cdots\text{N}$ ,  $\text{Cu}\cdots\text{F}$ ,  $\text{Cu}\cdots\text{L}\cdots\text{Cu}$ , and Axial  $\text{F}\cdots\text{SiF}_4\cdots\text{Axial F}$  to determine distance variations.

**Table 2. 1 Calculated Bond Distances for Synthesized MOMs**

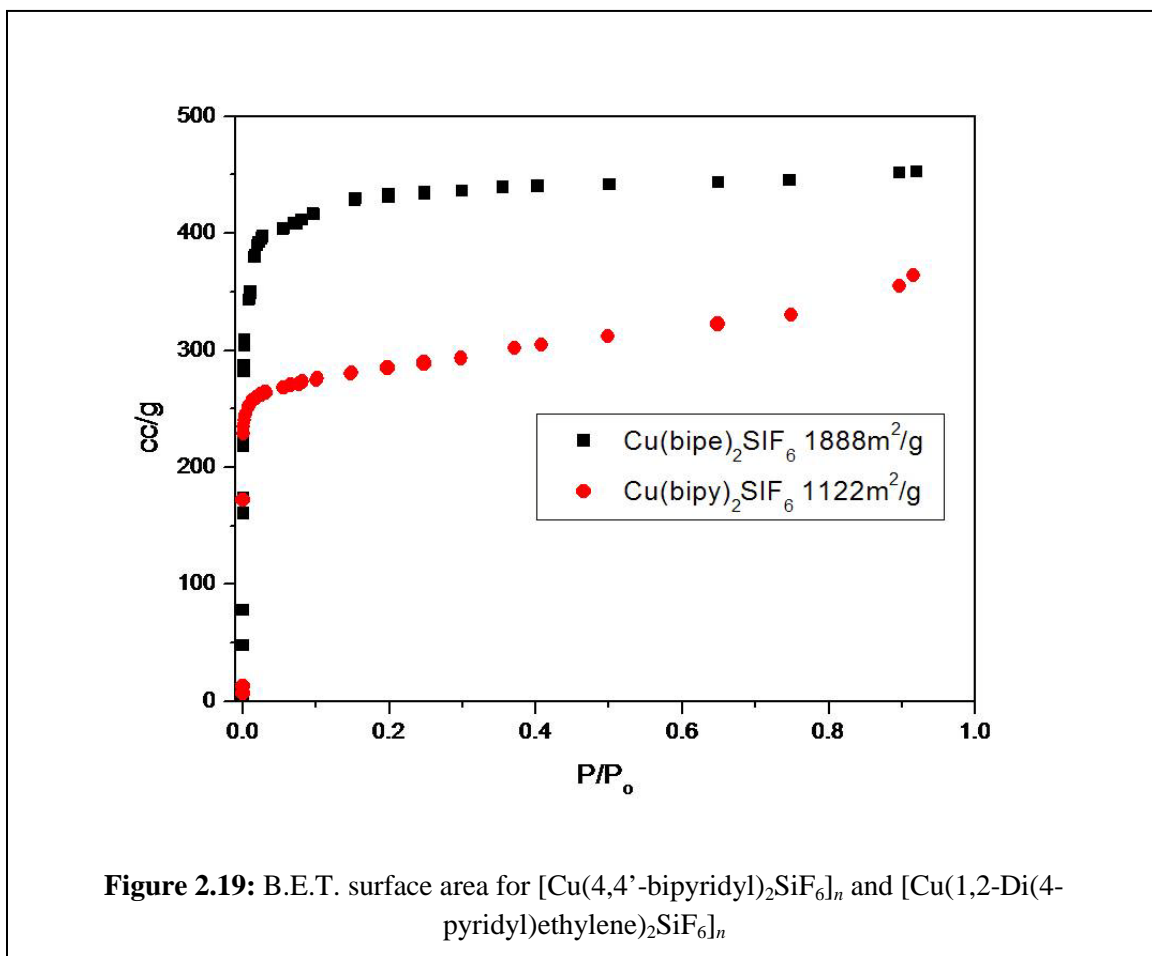
Bond	[1]	[2]	[3]
Cu····N <sub>d</sub> (Å)	2.0390	2.1572(2)	2.009(1)
Cu····F <sub>d</sub> (Å)	2.3565	2.08(1)	2.3760(1)
Cu····L····Cu	6.8520	11.396(1)	13.3615(1)
Axial F····SiF <sub>4</sub> ···· Axial F	8.1110	7.6775(9)	7.9931(2)

The bond distances between **1** and **3** were relatively equal for both the copper-nitrogen and copper-fluoride distance. However, structure **2** showed vast differences as compared to **1** and **3** with the copper-nitrogen bond being approximately 0.15 Å longer and the copper-fluoride bond approximately 0.3 Å shorter. The window size, or distance from Cu····L····Cu, was as expected, increased with increase ligand length. This variation in window size will allow for systematic evaluations of ligand length effects upon gas sorption and gas diffusion.

### 2.5.3 Determination of Surface Area from Nitrogen Isotherm

Surface areas of the synthesized MOMs were found using a Quantachrome NOVA 2000 and a multipoint B.E.T. obtained from nitrogen isotherms. Samples are exchanged with methanol before placement under vacuum to remove solvent molecules from the interior of the MOM. Using liquid nitrogen, N<sub>2</sub> is pumped into the sample cell at determined pressures containing the MOM. N<sub>2</sub> is physisorbed onto the surfaces of the MOM to determine the surface area. **Figure 2.19** represents the N<sub>2</sub> Isotherms for [Cu(4,4'-bipyridyl)<sub>2</sub>SiF<sub>6</sub>]<sub>n</sub> and [Cu(1,2-Di(4-pyridyl)ethylene)<sub>2</sub>SiF<sub>6</sub>]<sub>n</sub> along with the calculated surface area. The surface area for [Cu(1,2-Di(4-pyridyl)ethylene)<sub>2</sub>SiF<sub>6</sub>]<sub>n</sub> was calculated 1888 m<sup>2</sup>/g as compared to the [Cu(4,4'-bipyridyl)<sub>2</sub>SiF<sub>6</sub>]<sub>n</sub> with a surface area of 1122 m<sup>2</sup>/g. The surface area for [Cu(pyrazine)<sub>2</sub>SiF<sub>6</sub>]<sub>n</sub> could not be determined due to N<sub>2</sub> being too large for the pore. The window size with van der

Waals consideration is 3.45 Å while the kinetic diameter of N<sub>2</sub> is 3.7 Å, making N<sub>2</sub> too large to diffuse in the pore.



## 2.6 Discussion

Three novel, isorecticular MOMs with *pcu* topology have been synthesized using various methodologies. A copper node coordinated with varying pyridine-based organic linkers formed pillared square grids that are permanently porous and water stable. Several novel structures were synthesized and characterized along with the desired products. One particular structure shown in **Figure 2.4** was capable of ion exchange with chloride ions and further investigation into uptake of phosphates, sulfates, perchlorates will continue to show future applications in waste removal from water sources.

The first pillared MOM using  $\text{CuSiF}_6$  and 4,4'-bipyridine was synthesized using modified literature results.<sup>18</sup> This structure showed a relatively high surface area of  $1122 \text{ m}^2/\text{g}$  and was heated to approximately  $170 \text{ }^\circ\text{C}$  before structural decomposition. Bond distances in  $[\text{Cu}(4,4'\text{-bipyridyl})_2\text{SiF}_6]_n$  did not match the patterns found in the other two synthesized MOMs however. This structure, represented as **[2]** in **Table 2. 1**, showed a  $0.15 \text{ \AA}$  increase in copper-nitrogen distance and a  $0.3 \text{ \AA}$  decrease in copper-fluoride distance when compared to **[1]** and **[3]**. Accordingly, the distance between the axial fluorides in the  $\text{SiF}_6$  were found to be significantly lower than structures **[1]** and **[3]** due to differences in electronegativity of ligands altering the bond distances.

$[\text{Cu}(1,2\text{-Di}(4\text{-pyrdiy})\text{ethylene})_2\text{SiF}_6]_n$  was the second structure to be synthesized. This particular structure showed the highest surface area with a B.E.T. of  $1888 \text{ m}^2/\text{g}$  and upon measurement with TGA, showed structural decomposition at  $150 \text{ }^\circ\text{C}$ . This structure shows an interesting property in being able to control the polycatenation versus pillared framework. Several investigations have taken place to see if concentrations and temperatures affected the conditions of which structure was formed. However, neither of these conditional variations formed any conclusive evidence for control of which structure was favored at which condition. It is now believed that time of heating might be the controlling factor in which structure is yielded and further investigations into this condition will follow.

The third and final synthesized structure used the pyrazine linker to form  $[\text{Cu}(\text{pyrazine})_2\text{SiF}_6]_n$ . This MOM was the only one unable to have a surface area determination due to the inability for  $\text{N}_2$  to fit in the pore of the framework. However, this framework should have a surface area determination using alternate gas sorption such as Ar,  $\text{CO}_2$ , or  $\text{H}_2$ . TGA showed decomposition of the framework at  $150 \text{ }^\circ\text{C}$ .

Future endeavors will explore the sorption and diffusion of gases within the material. Gas sorption using  $\text{CO}_2$ ,  $\text{H}_2$  and  $\text{CH}_4$  will be investigated to have comparative studies on the effect of pore size on gas uptake. Furthermore,  $\text{H}_2$  diffusion will be investigated for the frameworks to also

determine the effect of pore size on gas diffusion. Also investigation into synthesizing a fourth pillared MOM using an extended pyridine based linker will take place to help develop the comparative study.

## **2.7 Experimental**

### ***2.7.1 Synthesis of $[Cu(4,4'-bipyridine)_2SiF_6]_n$***

0.2 mmol (41.1 mg)  $CuSiF_6$  was dissolved in 2 mL MeOH and added to a solution of 0.4 mmol (62.5 mg) 4,4'-bipyridine dissolved in 4 mL MeOH. Purple precipitate forms instantaneously. Percent yields were in excess of 60% per reaction.

### ***2.7.2 Synthesis of $\{[Cu(1,2-Di(4-pyridyl)ethylene)_2(H_2O)_2](SiF_6)(H_2O)\}_n$***

0.2 mmol (41.1 mg)  $CuSiF_6$  was dissolved in 2 mL  $H_2O$  and added to a solution of 0.4 mmol (72.9 mg) 1,2-Di(4-pyridyl)bipyethylene dissolved in 4 mL MeOH. The solution was heated at 85°C for 24 hr. Blue-gray crystals were yielded. Percent yields were in excess of 85% per reaction.

### ***2.7.3 Synthesis of $[Cu(1,2-Di(4-pyridyl)ethylene)_2SiF_6]_n$***

0.1 mmol (20.5 mg)  $CuSiF_6$  was dissolved in 2 mL  $H_2O$  and added to a solution of 0.2 mmol 1,2-Di(4-pyridyl)ethylene dissolved in 2 mL MeOH with 250  $\mu$ L nitrobenzene. The solution was heated at 85 °C for 24 hr. Purple crystals were yielded after 1 week. Percent yields were in excess of 70% per reaction.

### ***2.7.4 Synthesis of $[Cu(pyrazine)(SiF_6)(H_2O)_2]$***

0.2 mmol (41.1 mg)  $CuSiF_6$  was dissolved in a 4 mL ethylene glycol:water 50:50 system and added to a solution of 0.4 mmol (32.0 mg) pyrazine dissolved in 4 mL ethylene glycol. Sky blue

needle crystals formed after 24 hr. at room temperature. Percent yields were found to be approximately 70% per reaction.

#### ***2.7.5 Synthesis of $\text{Cu}(3,5\text{-lutidine})_4\text{SiF}_6$***

0.05 mmol (10.3 mg)  $\text{CuSiF}_6$  was dissolved in 1 mL  $\text{H}_2\text{O}$  and layered onto a solution of 0.1 mmol (8.0 mg) pyrazine dissolved in 1 mL MeOH with 50  $\mu\text{L}$  3,5-lutidine guest. Long purple needle-like crystals formed after 1 week. Percent yield was in excess of 80% per reaction.

#### ***2.7.6 Synthesis of $\text{Cu}(\text{pyrazine})_2(\text{SiF}_6)(\text{H}_2\text{O})$***

Slow diffusion of a solution of 0.1 mmol (20.5 mg)  $\text{CuSiF}_6$  dissolved in 2 mL MeOH onto 0.2 mmol (16.0 mg) pyrazine dissolved in 2 mL ethylene glycol. Blue crystals were yielded after 1 week. Reactions gave a percent yield upwards of 60% per reaction.

#### ***2.7.7 Synthesis of $[\text{Cu}(\text{pyrazine})_2\text{SiF}_6]_n$***

1.0 mmol (205.6 mg)  $\text{CuSiF}_6$  was dissolved in 10 mL MeOH and added to a solution of 2.0 mmol (160.2 mg) pyrazine in 10 mL ethylene glycol and heated at 85 °C for 24 hr. A teal precipitate formed after heating. Percent yields were in excess of 80% per reaction.

### **2.8 Conclusions**

This project entailed synthesizing three MOMs to be tested for gas diffusion and gas sorption. All three MOMs were constructed using a copper node, hexafluorosilicate pillaring agent, and a pyridine based organic linker. Each material was characterized by XRPD and TGA. Furthermore, each Cu-MOM was water and air stable giving it promise for applications in the real world.  $\text{H}_2$  gas diffusion studies will show the affect of pore size on diffusion through the

framework. With an expected high  $Q_{st}$  these materials could show promising applications in hydrogen fuels due to their stability, simple synthesis, and low cost. Also with their high surface area, these materials will be excellent candidates for the removal and storage of CO<sub>2</sub>, CH<sub>4</sub>, and other environmentally toxic gas and small molecules. Future investigations will show the uptake of varying gas molecules and a comparative study will be made to determine the affect of pore size with gas uptake.

Thus, as supramolecular chemistry and crystal engineering advance, so will the complexity and applicability of new materials. The beginning of the end for MOMs has been reached as accurate prediction capabilities have increased and vastly different materials with specific properties are being synthesized to suit an ever growing demand for clean energy. Scientists are coming ever closer to realizing Feynman's dream through simulated and experimental procedures that state specific conditions to develop desired products. Once this point is reached, the chemical world will see an explosion of materials with infinite possibilities in solving the world's energy and environmental needs. MOMs are the forefront of this age of discovery, and their potential is only just beginning to be tapped.

## References

- (1) Feynman, R. P. *The Feynman lectures on physics: Exercises*; Addison-Wesley Pub. Co., 1964.
- (2) Maddox, J. *Nature* **1988**, 335, 201.
- (3) Lehn, J. M. *Angewandte Chemie-International Edition in English* **1988**, 27, 89.
- (4) Lehn, J. M. *Supramolecular chemistry: concepts and perspectives*; VCH, 1995.
- (5) Fischer, E. *Berichte der deutschen chemischen Gesellschaft* **1894**, 27, 2985.
- (6) Werner, A. *Zeitschr. Anorg. Chem.* **1893**, 3, 267.
- (7) Wolf, K. L.; Wolff, R. *Angewandte Chemie* **1949**, 61, 191.

- (8) Pauling, L. *The nature of the chemical bond and the structure of molecules and crystals: an introduction to modern structural chemistry*; Cornell University Press, 1960.
- (9) Watson, J. D.; Crick, F. H. C. *Nature* **1953**, *171*, 737.
- (10) Desiraju, G. R. *Crystal engineering: the design of organic solids*; Elsevier, 1989.
- (11) Etter, M. C.; Adsmond, D. A. *Journal of the Chemical Society-Chemical Communications* **1990**, 589.
- (12) Desiraju, G. R. *Crystal design: structure and function*; Wiley, 2003.
- (13) Desiraju, G. R.; Steiner, T. *The weak hydrogen bond: in structural chemistry and biology*; Oxford University Press, 2001.
- (14) Gable, R. W.; Hoskins, B. F.; Robson, R. *Journal of the Chemical Society-Chemical Communications* **1990**, 1677.
- (15) Hoskins, B. F.; Robson, R. *Journal of the American Chemical Society* **1990**, *112*, 1546.
- (16) Kitagawa, S.; Kitaura, R.; Noro, S. *Angewandte Chemie-International Edition* **2004**, *43*, 2334.
- (17) Kitagawa, S.; Uemura, K. *Chemical Society Reviews* **2005**, *34*, 109.
- (18) Noro, S.; Kitagawa, S.; Kondo, M.; Seki, K. *Angewandte Chemie-International Edition* **2000**, *39*, 2082.
- (19) Biradha, K.; Fujita, M. *Chemical Communications* **2001**, 15.
- (20) Biradha, K.; Fujita, M. *Angewandte Chemie-International Edition* **2002**, *41*, 3392.
- (21) Biradha, K.; Hongo, Y.; Fujita, M. *Angewandte Chemie-International Edition* **2000**, *39*, 3843.
- (22) Biradha, K.; Hongo, Y.; Fujita, M. *Angewandte Chemie-International Edition* **2002**, *41*, 3395.
- (23) Kasai, K.; Aoyagi, M.; Fujita, M. *Journal of the American Chemical Society* **2000**, *122*, 2140.
- (24) Kofenstein, R.; Robl, C. *Zeitschrift Fur Anorganische Und Allgemeine Chemie* **2005**, *631*, 1035.
- (25) Kofenstein, R.; Robl, C. *Zeitschrift Fur Anorganische Und Allgemeine Chemie* **2005**, *631*, 1756.
- (26) Rather, B.; Zaworotko, M. J. *Chemical Communications* **2003**, 830.

- (27) Robinson, F.; Zaworotko, M. J. *Journal of the Chemical Society-Chemical Communications* **1995**, 2413.
- (28) Subramanian, S.; Zaworotko, M. J. *Angewandte Chemie-International Edition in English* **1995**, *34*, 2561.
- (29) Lin, M. J.; Jouaiti, A.; Kyritsakas, N.; Hosseini, M. W. *Crystengcomm* **2009**, *11*, 189.
- (30) Lin, M. J.; Jouaiti, A.; Kyritsakas, N.; Hosseini, M. W. *Crystengcomm* **2011**, *13*, 776.
- (31) Chui, S. S.-Y.; Lo, S. M.-F.; Charmant, J. P. H.; Orpen, A. G.; Williams, I. D. *Science* **1999**, *283*, 1148.
- (32) Li, H.; Eddaoudi, M.; O'Keeffe, M.; Yaghi, O. M. *Nature* **1999**, *402*, 276
- (33) Wells, A. F. *Structural inorganic chemistry*; Clarendon Press, 1975.
- (34) Furukawa, H.; Ko, N.; Go, Y. B.; Aratani, N.; Choi, S. B.; Choi, E.; Yazaydin, A. O.; Snurr, R. Q.; O'Keeffe, M.; Kim, J.; Yaghi, O. M. *Science* **2010**, *329*, 424.
- (35) Fujita, M.; Kwon, Y. J.; Washizu, S.; Ogura, K. *Journal of the American Chemical Society* **1994**, *116*, 1151.